Atmos. Meas. Tech., 8, 2555–2576, 2015
www.atmos-meas-tech.net/8/2555/2015/
doi:10.5194/amt-8-2555-2015

Atmospheric Measurement Techniques Open Access

ACTRIS ACSM intercomparison – Part 2: Intercomparison of ME-2 organic source apportionment results from 15 individual, co-located aerosol mass spectrometers

R. Fröhlich[1], V. Crenn[2], A. Setyan[3], C. A. Belis[4], F. Canonaco[1], O. Favez[5], V. Riffault[3], J. G. Slowik[1], W. Aas[6], M. Aijälä[7], A. Alastuey[8], B. Artiñano[9], N. Bonnaire[2], C. Bozzetti[1], M. Bressi[4], C. Carbone[10], E. Coz[9], P. L. Croteau[11], M. J. Cubison[12], J. K. Esser-Gietl[13], D. C. Green[14], V. Gros[2], L. Heikkinen[7], H. Herrmann[15], J. T. Jayne[11], C. R. Lunder[6], M. C. Minguillón[8], G. Močnik[16], C. D. O'Dowd[17], J. Ovadnevaite[17], E. Petralia[18], L. Poulain[15], M. Priestman[14], A. Ripoll[8], R. Sarda-Estève[2], A. Wiedensohler[15], U. Baltensperger[1], J. Sciare[2,19], and A. S. H. Prévôt[1]

[1]Laboratory of Atmospheric Chemistry, Paul Scherrer Institute, Villigen PSI, Switzerland
[2]Laboratoire des Sciences du Climat et de l'Environnement, LSCE, CNRS-CEA-UVSQ, Gif-sur-Yvette, France
[3]Ecole Nationale Supérieure des Mines de Douai, Département Sciences de l'Atmosphère et Génie de l'Environnement, Douai, France
[4]European Commission, Joint Research Centre, Institute for Environment and Sustainability, Ispra (VA), Italy
[5]INERIS, Verneuil-en-Halatte, France
[6]NILU – Norwegian Institute for Air Research, Kjeller, Norway
[7]Department of Physics, University of Helsinki, Helsinki, Finland
[8]Institute of Environmental Assessment and Water Research (IDAEA-CSIC), Barcelona, Spain
[9]Centre for Energy, Environment and Technology Research (CIEMAT), Department of the Environment, Madrid, Spain
[10]Proambiente S.c.r.l., CNR Research Area, Bologna, Italy
[11]Aerodyne Research, Inc., Billerica, Massachusetts, USA
[12]TOFWERK AG, Thun, Switzerland
[13]Deutscher Wetterdienst, Meteorologisches Observatorium Hohenpeißenberg, Hohenpeißenberg, Germany
[14]Environmental Research Group, MRC-HPA Centre for Environment and Health, King's College London, London, UK
[15]Leibniz Institute for Tropospheric Research, Leipzig, Germany
[16]Aerosol d.o.o., Ljubljana, Slovenia
[17]School of Physics and Centre for Climate and Air Pollution Studies, Ryan Institute, National University of Ireland Galway, Galway, Ireland
[18]ENEA-National Agency for New Technologies, Energy and Sustainable Economic Development, Bologna, Italy
[19]The Cyprus Institute, Environment Energy and Water Research Center, Nicosia, Cyprus

Correspondence to: A. S. H. Prévôt (andre.prevot@psi.ch)

Received: 24 December 2014 – Published in Atmos. Meas. Tech. Discuss.: 4 February 2015
Revised: 8 May 2015 – Accepted: 29 May 2015 – Published: 24 June 2015

Abstract. Chemically resolved atmospheric aerosol data sets from the largest intercomparison of the Aerodyne aerosol chemical speciation monitors (ACSMs) performed to date were collected at the French atmospheric supersite SIRTA. In total 13 quadrupole ACSMs (Q-ACSM) from the European ACTRIS ACSM network, one time-of-flight ACSM (ToF-ACSM), and one high-resolution ToF aerosol mass spectrometer (AMS) were operated in parallel for about 3 weeks in November and December 2013. Part 1 of this study reports on the accuracy and precision of the instruments for all the measured species. In this work we report on the intercomparison of organic components and the results from factor analysis source apportionment by positive matrix factorisation (PMF) utilising the multilinear engine 2 (ME-2).

Published by Copernicus Publications on behalf of the European Geosciences Union.

Except for the organic contribution of mass-to-charge ratio m/z 44 to the total organics (f_{44}), which varied by factors between 0.6 and 1.3 compared to the mean, the peaks in the organic mass spectra were similar among instruments. The m/z 44 differences in the spectra resulted in a variable f_{44} in the source profiles extracted by ME-2, but had only a minor influence on the extracted mass contributions of the sources. The presented source apportionment yielded four factors for all 15 instruments: hydrocarbon-like organic aerosol (HOA), cooking-related organic aerosol (COA), biomass burning-related organic aerosol (BBOA) and secondary oxygenated organic aerosol (OOA). ME-2 boundary conditions (profile constraints) were optimised individually by means of correlation to external data in order to achieve equivalent / comparable solutions for all ACSM instruments and the results are discussed together with the investigation of the influence of alternative anchors (reference profiles). A comparison of the ME-2 source apportionment output of all 15 instruments resulted in relative standard deviations (SD) from the mean between 13.7 and 22.7 % of the source's average mass contribution depending on the factors (HOA: 14.3 ± 2.2 %, COA: 15.0 ± 3.4 %, OOA: 41.5 ± 5.7 %, BBOA: 29.3 ± 5.0 %). Factors which tend to be subject to minor factor mixing (in this case COA) have higher relative uncertainties than factors which are recognised more readily like the OOA. Averaged over all factors and instruments the relative first SD from the mean of a source extracted with ME-2 was 17.2 %.

1 Introduction

Measurements have shown that organic compounds constitute a major fraction of the total particulate matter (PM) all around the world (20–90 % of the submicron aerosol mass according to Kanakidou et al., 2005). Elevated concentrations of organic aerosols due to anthropogenic activities are a major contributor to the predominantly adverse effects of aerosols on climate (Lohmann and Feichter, 2005; Stevens and Feingold, 2009; Boucher et al., 2013; Carslaw et al., 2013), weather extremes (Wang et al., 2014a, b), Earth's ecosystem (Mercado et al., 2009; Carslaw et al., 2010; Mahowald, 2011) or on human health (Seaton et al., 1995; Laden et al., 2000; Cohen et al., 2005; Pope and Dockery, 2006). According to recent estimates of the global burden of disease, up to 3.6 million (Lim et al., 2013) of the about 56 million annual deaths (Mathers et al., 2005) were connected to ambient particulate air pollution in the year 2010. These numbers underline the importance of detailed knowledge about the sources of ambient aerosols to be able to efficiently reduce air pollution levels.

Positive matrix factorisation (PMF), a statistical factor analysis algorithm developed by Paatero and Tapper (1994) and Paatero (1997), is a widely and successfully used approach to simplify interpretation of complex data sets by representing measurements as a linear combination of static factor profiles and their time-dependent intensities (Lanz et al., 2007, 2010; Ulbrich et al., 2009; Crippa et al., 2014). The multilinear engine implementation (ME-2, Paatero, 1999) allows for the introduction of additional constraints (e.g. external factor profiles) to the algorithm. The algorithm has been heavily used for source identification and quantification with organic mass spectra measured by the Aerodyne aerosol mass spectrometer (AMS, Jayne et al., 2000; Drewnick et al., 2005; DeCarlo et al., 2006) and the related aerosol chemical speciation monitor (ACSM, Ng et al., 2011c; Fröhlich et al., 2013). Typically, the organic fraction of PM can be split up in primary (POA) and secondary organic aerosol (SOA). Origin and precursors of the SOA, which often can be separated according to volatility into a more oxidised (low-volatility LV-OOA) and a less oxidised fraction ("semi"-volatility SV-OOA) (Jimenez et al., 2009; Ng et al., 2010) remain largely unclear (Hallquist et al., 2009). Conversely, many POA sources have been identified (Zhang et al., 2011): hydrocarbon-like organic aerosol (HOA, Zhang et al., 2005a, b), biomass burning-related organic aerosol (BBOA, Alfarra et al., 2007; Aiken et al., 2010), cooking-related organic aerosol (COA, Slowik et al., 2010; Allan et al., 2010; Mohr et al., 2012; Canonaco et al., 2013; Crippa et al., 2014, 2013a), coal burning-related organic aerosol (CBOA, Hu et al., 2013b; Huang et al., 2014), nitrogen-enriched OA (NOA, Sun et al., 2011; Aiken et al., 2009) or local sources of primary organics (Timonen et al., 2013; Faber et al., 2013). Another marine source of secondary organic aerosol (MOA) related to MSA was reported by Crippa et al. (2013b).

Like every measurement or model, the results of PMF/ME-2 are subject to uncertainties. These uncertainties may result from the mathematical model itself (Paatero et al., 2014) or from the measurement technique applied. Within a certain measurement technique the effects of basic instrument precision, e.g. calculation of the measurement uncertainty matrix, can be distinguished from systematic differences between instruments outside of measurement precision. The latter will be investigated in this study for the first time on a large basis of 15 co-located, individual aerosol mass spectrometers employing the same experimental technique ($13 \times$ Q-ACSM, $1 \times$ ToF-ACSM, $1 \times$ HR-ToF-AMS). By comparing the source apportionment results of these 15 individual instruments, previously operated at different stations all over Europe (see http://psi.ch/ZzWd), a measure of comparability of PMF results across data sets recorded by different instruments is obtained.

Especially in the light of the growing number of ACSMs in Europe (promoted by the ACTRIS project: Aerosols, Clouds, and Trace gases Research InfraStructure network) and other parts of the world a better evaluation and understanding of the uncertainties of this technique in terms of concentrations (part 1 of this study, Crenn et al., 2015) and source apportionment (this paper) is needed. Large intercomparison cam-

paigns under real ambient conditions like the presented one are insightful and necessary exercises to ensure data quality and comparability of ACSM measurements.

2 Methodology and instrument description

The 15 Aerodyne mass spectrometers, which were provided by the co-authoring institutions (see Table S1 in the Supplement) will be denoted herein as #1–#13 (Q-ACSMs), ToF (ToF-ACSM) and HR(-AMS) (HR-ToF-AMS). The data sets were recorded during the ACTRIS ACSM intercomparison campaign taking place during 3 weeks in November and December 2013 at the SIRTA (Site Instrumental de Recherche par Télédétection Atmosphérique) station of the LSCE (Laboratoire des sciences du climat et l'environnement) in Gif-sur-Yvette, in the region of Paris (France), now hosting the European Aerosol Chemical Speciation Monitor Calibration Centre (ACMCC) which is part of the ACTRIS European Center for Aerosol Calibration. Detailed results of the intercomparison can be found in part 1 of this study (Crenn et al., 2015). For this intercomparison study data between 16 November and 1 December were considered (the full period of parallel measurements of all instruments).

2.1 Site description

SIRTA is a well-established atmospheric observatory in the vicinity of the French megacity Paris. The measurement site is located on the plateau of Saclay on the campus of CEA (French Alternative Energies and Atomic Energy Commission) at "Orme des Merisiers" (48.709° N, 2.149° E, 163 m a.s.l.). Being approximately 20 km southwest of the city centre of Paris, the station is classified as regional background, surrounded mainly by agricultural fields, forests, small villages and other research facilities. The closest major road is located about 2 km northeast. Overviews of wintertime aerosol sources and composition in the Paris region can be found in Crippa et al. (2013a) and Bressi et al. (2014).

All 15 instruments were located in the same laboratory, distributed to five separate $PM_{2.5}$ inlets on the roof of the building. A suite of additional aerosol and gas phase instruments (e.g. an Aethalometer for source apportionment of black carbon – for a complete list and description of the inlets and collocated instruments refer to Crenn et al., 2015) were operated in parallel, providing important data facilitating the validation of sources identified in this study.

2.2 Aerosol mass spectrometers

The focus of this work lies on source apportionment performed on data recorded with three different but related types of aerosol mass spectrometer: the high-resolution time-of-flight aerosol mass spectrometer (HR-ToF-AMS) was running alternatively in V- and W-mode every 2 min, recording aerosol spectra with a mass resolution of up to $\frac{M}{\Delta M} =$ 5000 (W-mode), the time-of-flight aerosol chemical speciation monitor (ToF-ACSM) operating at 10 min intervals with a resolution of $\frac{M}{\Delta M} = 600$ and the quadrupole aerosol chemical speciation monitor (Q-ACSM) with unit mass resolution (UMR) and time steps of ~ 30 min. All three instruments employ the same operational principle. Aerosol particles are focused into a vacuum chamber by an aerodynamic lens (Liu et al., 1995a, b, 2007; Zhang et al., 2004) where they are separated from the gas molecules as effectively as possible by a skimmer cone. These particles are flash vaporised on a heated (600 °C) inverted cone of porous tungsten. The resulting gas is then ionised by electron impact (~ 70 eV) and detected by the different ion mass spectrometers (Tofwerk HTOF, Tofwerk ETOF, Pfeiffer Prisma Plus QMG 220 quadrupole). While in the quadrupole mass spectrometer the m/z (mass-to-charge) channels are scanned through at a limited speed of typically 200 ms amu^{-1} (32 data points per amu); the TOF systems measure all ions at every extraction and provide a generally greater mass-to-charge resolving power and sensitivity. Vaporisation can induce thermal decomposition, while electron impact ionisation leads to extensive fragmentation. Both processes reduce the amount of available molecular information. Using fragmentation patterns known from controlled laboratory experiments (Allan et al., 2004; Aiken et al., 2008) allows for the determination of the main non-refractory aerosol species (nitrate, sulfate, ammonium, chloride and bulk organic matter).

Each instrument sampled dried aerosol at a similar flow rate of 0.1 L min^{-1} with an additional bypass flow of 2.9 L min^{-1} to reduce particle losses in the lines. Small possible variations of the flows between instruments are taken into account by the standard air beam correction routinely performed on AMS and ACSM data. In the AMS and ACSM systems mass spectral backgrounds must be recorded and this is done differently between the two instruments. The AMS systems use a chopper slit-wheel inside the vacuum chamber to alternate between measurements of aerosol and chamber background (i.e. the particle beam is fully blocked), the ACSM systems use an automated three-way valve switch assembly. This valve is periodically switched between two lines: the air in one line was filtered ("background") while the other line carries ambient, particle-laden air. All necessary calibrations (ionisation efficiency of nitrate (IE), relative ionisation efficiencies (RIE) of ammonium and sulfate, mass-to-charge axis (m/z), lens alignment, volumetric flow into the vacuum chamber, detector amplification (for more details we refer to the respective publications or the review of Canagaratna et al., 2007) were performed and monitored on site by the same operators using the same calibration equipment (e.g. SMPS). Since this study is mainly focused on a relative intercomparison of the ME-2 source apportionment, a constant collection efficiency of CE = 0.5 (Huffman et al., 2005; Matthew et al., 2008) was assumed for all instruments (for a more detailed analysis see Crenn et al., 2015).

The following software packages were used. Q-ACSM: version 1.4.4.5. of the ACSM DAQ software (Aerodyne Research Inc., Billerica, Massachusetts) during data acquisition and version 1.5.3.2 of the ACSM local tool (Aerodyne Research Inc., Billerica, Massachusetts) for Igor Pro (Wavemetrics Inc., Lake Oswego, Oregon) for Q-ACSM data treatment and export of PMF matrices (see Supplement for discussion of changes in most recent software version 1.5.5.0). ToF-ACSM: TOFDAQ version 1.94 (TOFWERK AG, Thun, Switzerland) during acquisition and Tofware version 2.4.2 (TOFWERK AG, Thun, Switzerland) for Igor Pro for data treatment. ToF-ACSM PMF matrices were calculated manually in accordance with the procedures employed in the AMS software SQUIRREL v1.52G (http://cires.colorado.edu/jimenez-group/ToFAMSResources/ToFSoftware/). AMS: standard ToF-AMS data acquisition software v4.0.24 (https://sites.google.com/site/tofamsdaq/) and the Thuner v1.5.10.0 (TOFWERK AG, Thun, Switzerland) to perform the automatic tuning of the ToF-MS voltages during acquisition were employed. Pika v1.12G (http://cires.colorado.edu/jimenez-group/ToFAMSResources/ToFSoftware/) was used for the high-resolution data analysis. The fragmentation table was adjusted according to recommendations (Aiken et al., 2008) in order to take into account air interferences and the water fragmentation pattern.

2.3 Aethalometer, NO_x analyser and PTR-MS

In the context of this paper, data from various external measurements, namely an Aethalometer, a NO_x analyser and a PTR-MS were used to validate factors found by the ME-2 source apportionment. The Magee Scientific Aethalometer model AE33 (Drinovec et al., 2015; Aerosol d.o.o., Ljubljana, Slovenia) measures black carbon (BC) aerosol by collecting aerosol on a filter and determining the light absorption at seven different wavelengths (Hansen et al., 1984). Potential sample loading artefacts detailed in Collaud Coen et al. (2010) are automatically compensated for according to the procedures described in Drinovec et al. (2015). The absorption coefficient b_{abs} depends on the wavelength λ and the Ångström exponent α_i, following the relationship

$$b_{abs} \propto \lambda^{-\alpha_i}. \quad (1)$$

By exploiting the wavelength dependence, i.e. the Ångström exponent is source-specific (Sandradewi et al., 2008), the measured BC can be separated into BC from wood burning (BC_{wb}) and BC from fossil fuel combustion (BC_{ff}). To this end a system of four equations has to be solved:

$$\frac{b_{abs}(\lambda_1)_{ff}}{b_{abs}(\lambda_2)_{ff}} = \left(\frac{\lambda_1}{\lambda_2}\right)^{-\alpha_{ff}} \quad (2)$$

$$\frac{b_{abs}(\lambda_1)_{wb}}{b_{abs}(\lambda_2)_{wb}} = \left(\frac{\lambda_1}{\lambda_2}\right)^{-\alpha_{wb}} \quad (3)$$

$$b_{abs}(\lambda_1)_{tot} = b_{abs}(\lambda_1)_{ff} + b_{abs}(\lambda_1)_{wb} \quad (4a)$$

$$b_{abs}(\lambda_2)_{tot} = b_{abs}(\lambda_2)_{ff} + b_{abs}(\lambda_2)_{wb} \quad (4b)$$

with absorption coefficients of wood burning and fossil fuel combustion $b_{abs,\,wb/ff}$ at two different wavelengths λ (here: $\lambda_1 = 470$ nm and $\lambda_2 = 880$ nm) and the corresponding Ångström exponents $\alpha_{wb/ff}$. According to literature α_{wb} typically lies between 1.9 and 2.2 (Sandradewi et al., 2008) and α_{ff} between 0.9 and 1.1 (Bond and Bergstrom, 2006). More recent studies suggested slightly lower α_{wb} of 1.6–1.7 (Saleh et al., 2013; Liu et al., 2014) but this does not affect the overall time trends used for the correlation with sources found by PMF. In agreement with the sensitivity analysis done by Sciare et al. (2011) for the Paris region, Ångström exponents of $\alpha_{wb} = 2$ and $\alpha_{ff} = 1$ were used in the BC source apportionment of this study. The fractions of BC emitted by the respective sources can then be calculated linearly from the total measured BC and the fraction of the corresponding absorption coefficient.

NO_x concentrations were measured by a photolytic NO-NO_2 analyser (model T200UP NO-NO_2, Teledyne API, San Diego, CA, USA) via ozone-induced chemiluminescence. Gaseous methanol and acetonitrile concentrations were detected by a proton-transfer-reaction mass spectrometerf (PTR-MS, serial # 10-HS02 079, Ionicon Analytik, Innsbruck, Austria, Hansel et al., 1995; Graus et al., 2010) which is described elsewhere (Sciare et al., 2011).

2.4 ME-2 and SoFi tool

For source apportionment (SA) of organic aerosol mass spectral data sets the methods of choice usually are 2-D bilinear models like PMF (Paatero and Tapper, 1994; Paatero, 1997) or chemical mass balance (CMB, Watson et al., 1997; Ng et al., 2011b). In particular, PMF has successfully been used in numerous AMS SA studies (Zhang et al., 2011). In both methods the organic $m \times n$ spectral matrix $\mathbf{X}$, containing m organic mass spectra (rows) with n ion fragments each (columns), is factorised into two submatrices, the profiles $\mathbf{F}$ and time series $\mathbf{G}$. The $\mathbf{F}$ is a $p \times n$ and $\mathbf{G}$ is an $m \times p$ matrix with p indicating the number of profiles. The residual $m \times n$ matrix $\mathbf{E}$ contains the fraction of $\mathbf{X}$ which is not explained by the current factorisation/model solution and is minimised by the PMF algorithm:

$$\mathbf{X} = \mathbf{GF} + \mathbf{E}. \quad (5)$$

Within the ME-2 package several cases of PMF are implemented: the traditional unconstrained PMF, PMF with controlled rotations (in many cases this is simply denoted "ME-2"), or fully constrained PMF (a form of CMB). While in unconstrained PMF the algorithm models the (entirely positive) profile and time series matrices $\mathbf{F}$ and $\mathbf{G}$ with a pre-set number of factors p by iteratively minimising the quantity

Q (main part of the object function as defined by Paatero and Hopke, 2009), the fully constrained (CMB-like) PMF algorithm needs well-defined factor profiles as input and attributes a time series of concentrations to them:

$$Q = \sum_{i=1}^{m}\sum_{j=1}^{n}\left(\frac{e_{ij}}{\sigma_{ij}}\right)^2 \quad (6)$$

with e_{ij} being the elements of the residual matrix **E** and σ_{ij} the measurement uncertainties of ion fragment j at time step i. In many cases, e.g. when two factors have similar time series (e.g. heating and cooking in the evening) or profiles (e.g. traffic and cooking, Mohr et al., 2009), the totally unconstrained PMF has difficulties separating these factors (this was already pointed out in former studies, e.g. by Sun et al., 2010). The multilinear engine (ME-2) provides additional control over the rotational ambiguity (Paatero and Hopke, 2009). Here the solution space is explored by introducing a priori information (e.g. factor profiles) for some (not necessary all) of the factors p. The strength of this additional constraint is set by the so-called a value (Paatero and Hopke, 2009; Brown et al., 2012), which determines how much deviation from the constraint profile the model allows. It ranges from zero to one and can be understood as the relative fraction – by how much each m/z may individually deviate from the a priori profile (Lanz et al., 2008). In that way, ME-2 covers the whole range of bilinear models from fully constrained ($a = 0$) to completely unconstrained PMF (no a value set). Moving away from the unconstrained solution typically leads to an increase in Q. The magnitude of this increase of Q is used in order to remove solutions whose rotations are not a mathematically adequate representation of the input data set. All factor analyses presented in this study were performed in the robust mode (Paatero, 1997).

Initialisation of the ME-2 engine and analysis of the results was performed using the source finder tool (SoFi v4.6, http://psi.ch/HGdP, Canonaco et al., 2013) package for Igor Pro (WaveMetrics Inc., Lake Oswego, Oregon).

2.5 Model input and data preparation

As an input, the ME-2 algorithm requires the organic data matrix, the associated error matrix, and the corresponding time and mass-to-charge (m/z) axis. For each instrument the input data were created up to m/z 100 and individually cleaned up. Bad data points were identified by standard diagnostics (airbeam signal, inlet pressure, voltage settings, etc.). A uniform CE = 0.5 and a uniform organics $\mathrm{RIE_{org}} = 1.4$ were used for all data sets. The corresponding ionisation efficiency (IE) or, more accurately for the Q-ACSMs, the response factor (RF) calibration values were determined during the first week of the intercomparison study on site (Crenn et al., 2015) and can be found in Table S2. Q-ACSM data were corrected for a decrease in ion transmission at high m/z ($\gtrsim$55) according to a standard curve obtained by Ng et al. (2011c). For further discussion and recent software updates concerning the relative ion transmission (RIT) calculation for PMF matrices refer to the discussion in the Supplement. To correct for the decay of the detector amplification the airbeam N_2 signal at m/z 28 was used (reference value: 1×10^{-7} A) maintaining the detectors at gain values of around 20 000.

The ToF-ACSM data set exhibited an unusual (exponentially decaying) drift in addition to the drift of the airbeam signals, visible in the always present background signals like the one of stable tungsten isotopes (originating from the ioniser filament). This indicates a change in the IE/AB ratio during the campaign which was confirmed by calibrations at the beginning and at the end. To avoid influence of potential real ambient aerosol trends, a correction function was deduced from the largest signals in the background (m/z 105, 130, 132, 182 and 221, see Fig. S1) and applied to the data set, making the assumption that the IE of ambient aerosol molecules is affected the same way as the molecules in the chamber background. This drift is attributed to transient effects in the electronics occurring after the replacement of the electron multiplier.

A probably too short delay time of the quadrupole scan after a valve switch (125 ms) caused physically not meaningful negative values at the signal channel of m/z 12, therefore the m/z 12 column was removed from all Q-ACSM matrices prior to PMF analysis. m/z channels with weak signals may influence the operation of the PMF algorithm and therefore also the solutions in a suboptimal way because the algorithm may try to apportion nonsensical noise. In order to avoid this the corresponding uncertainty of weak channels can be increased to reduce their weight according to Eq. (6). Table S3 shows a list of down-weighted m/z channels for each instrument. The decision as to whether a channel was down-weighted or not was made individually either because of low signal-to-noise ratio according to the recommendations of Ulbrich et al. (2009) or because of spotted outliers with high weighted residuals. Furthermore, the uncertainties of m/z channels that are not directly measured but recalculated from fractions of the signal at m/z 44 via the fragmentation table (Allan et al., 2004) are adjusted as well according to the recommendation of Ulbrich et al. (2009).

2.6 Optimisation of ME-2 constraints

Optimal a values in each case were determined by systematic variation of the a value in relation to increases or decreases of the correlation coefficient R^2 of the factor time series with external tracers. The correlations that were maximised for the determination of the best a values were: BBOA factor with $\mathrm{BC_{wb}}$, OOA factor with inorganic $\mathrm{SO_4}$ (covariance of OOA with sulfate was found at the SIRTA site before by Crippa et al., 2013a) and HOA factor with $\mathrm{BC_{ff}}$ and NO_x. Correlation maxima (R^2) are listed in Table 1. Changes in a value usually affected mainly the cor-

Table 1. Coefficients of determination (R^2) between the factors of each instrument's best ME-2 solution (left column of Table 2) and external measurements.

R^2	BBOA / BC_{wb}	HOA / BC_{ff}	HOA / NO_x	OOA / SO_4
ToF	0.91	0.69	0.77	0.66
#1	0.94	0.64	0.66	0.60
#2	0.93	0.67	0.62	0.52
#3	0.91	0.71	0.65	0.70
#4	0.93	0.73	0.75	0.61
#5	0.85	0.66	0.62	0.75
#6	0.87	0.57	0.55	0.76
#7	0.87	0.58	0.53	0.72
#8	0.87	0.59	0.61	0.79
#9	0.86	0.71	0.69	0.76
#10	0.90	0.55	0.56	0.77
#11	0.85	0.52	0.52	0.75
#12	0.87	0.59	0.59	0.78
#13	0.85	0.65	0.65	0.66
HR-AMS	0.90	0.68	0.65	0.51

relations of the HOA factor while the correlations of the BBOA and OOA factors were quite stable. On that account two correlations to HOA were made. The sum of the two HOA R^2 was maximised. For COA no reliable external tracer was measured. For all factors good correlations with the respective external measurement were reached: $BBOA/BC_{wb}$: median $R^2 = 0.87$ (range 0.85–0.94), HOA/BC_{ff}: median $R^2 = 0.65$ (range 0.52–0.73), HOA/NO_x: median $R^2 = 0.62$ (range 0.52–0.77), OOA/SO_4: median 0.72 (range 0.51–0.79).

The applied strategy was: increase of a in steps of $\Delta a = 0.05$ until a maximum R^2 (coefficient of correlation between time series of resulting factors and corresponding external tracers) is found. If two factor profiles are constrained, first both a values are varied simultaneously until a maximum R^2 is found. From this point, the a value of one of reference profiles is varied independently in both directions (smaller and larger a values) while the a value of the other reference profile stays constant. Again after a maximum R^2 is found, the a value of the other reference profile is varied, looking for the maximal correlation with external data (see flowchart in Fig. S8). In this way a large range of a values could be explored for each instrument.

It is to note that of course also the BC source apportionment and other external data used for this sensitivity analysis are prone to uncertainties. The approach detailed above therefore should, if applied elsewhere, always be used with caution, and a sensitivity analysis on the dependence of the results on the input model parameters should be performed. In the presented case the optimisation of a values assured the comparability of the 15 solutions used for the intercomparison of the ME-2 method. A thorough discussion of the uncertainties of the BC source apportionment method and a comparison to other source apportionment methods can be found in Favez et al. (2010).

3 Results

In the discussion below the 13 participating Q-ACSMs in this study are denoted "#1" to "#13" while the ToF-ACSM will be denoted "ToF" and the HR-ToF-AMS "HR", following the notation of the companion paper of Crenn et al. (2015). A complete list of the participating instruments can be found in Table S1. Times are presented in local time (CET = UTC + 1 h).

3.1 Organic time series

Figure 1 shows the time traces of bulk organic matter during the 16 days of simultaneous measurement used for the subsequent ME-2 analysis (16 November–1 December 2013, this corresponds to 550–780 data points depending on data availability of each instrument). The median organic concentration calculated on a point-by-point basis of the 13 Q-ACSMs is displayed as a black line with the interquartile range (IQR) (25–75 percentile) shaded in red and the 10–90 percentile range shaded in grey. The ToF-ACSM time series is shown in green and the AMS in pink. Correlations of ToF-ACSM and AMS with the median of the Q-ACSMs is shown in the two inset graphs. Good qualitative and quantitative agreement between all 15 aerosol mass spectrometers was achieved ($R^2 = 0.82$–0.99, slope = 0.70–1.37, see Crenn et al., 2015 for intercomparison between Q-ACSMs or Fig. 1 for comparison of Q-ACSMs to HR-AMS and ToF-ACSM). Average organic matter concentrations during the whole period with 6.9 µg m^{-3} (range ≈ 0.7–25 µg m^{-3}) were in the range of typical OA concentrations at this site (Petit et al., 2015), providing good boundary conditions (high signal-to-noise and variability) for PMF source apportionment. For a more detailed analysis of the concentration ranges we refer to Crenn et al. (2015).

3.2 Organic mass spectra

The mass spectrometer discriminates molecular fragments of certain mass-to-charge ratios. The data are then typically displayed as stick plots containing the respective signals for each m/z. The bulk organic signal is calculated from the sum of the sticks (total integrated signal for a given integer m/z) associated with organic molecules or molecular fragments according to known fragmentation patterns detailed in Allan et al. (2004). This is done under the assumption that with constant boundary conditions the fragmentation is constant as well. The sticks in Fig. 2a represent the median fractions of total organic matter at the respective mass-to-charge ratios for the 13 Q-ACSM instruments during an interruption-free 20 h period (26 November 10:00–27 November 06:00 LT, UTC + 1 h). The IQR and the full range are displayed as boxes and whiskers respectively.

There is significant information remaining in the organic molecular fragments. For example fragments at m/z 60

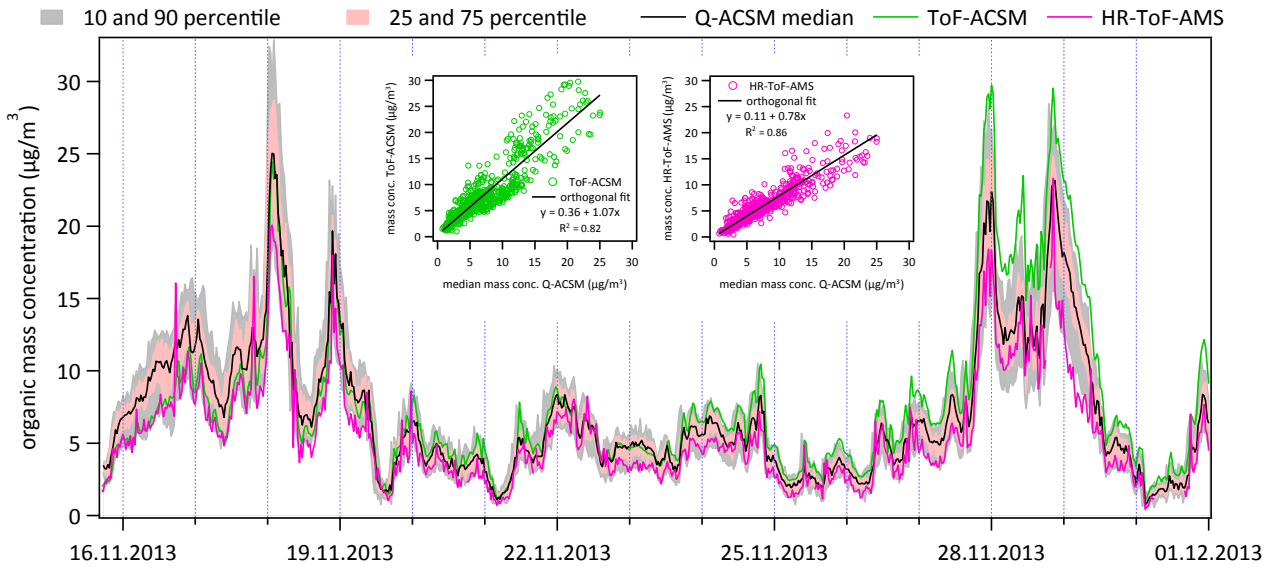

Figure 1. Time series of bulk organic matter for all 15 instruments in µg m^{-3} (CE = 0.5, RIE$_{org}$ = 1.4). The green trace shows organic matter measured by the ToF-ACSM, the pink trace HR-ToF-AMS organic matter and the black trace the median of organic matter measured by the 13 Q-ACSMs. Since all ACSMs run with slightly different time steps all data shown in this plot had to be re-gridded to the same 30 min timescale for the calculation of median and inter-percentile ranges. The light red and light grey regions indicate the 25–75 percentile range and the 10–90 percentile range of the Q-ACSM measurements, respectively. The two small insets show the correlation between ToF-ACSM and median Q-ACSM organic (green) and the same for HR-ToF-AMS and median Q-ACSM (pink). Slopes and coefficients of determination of an orthogonal distance regression are given in the plots. Average organic matter concentrations during the whole period were 6.9 µg m^{-3}.

(mainly $C_2H_4O_2^+$) and m/z 73 ($C_3H_5O_2^+$) mostly originate from primary biomass burning particles (Alfarra et al., 2007; Ng et al., 2010; Cubison et al., 2011). There are exceptions in marine environments where the signal at m/z 60 can also be mainly from $Na^{37}Cl$, see Ovadnevaite et al. (2012). m/z 29 (mainly CHO^+) as well is often enhanced in wood burning emissions but is also observed from other sources e.g. SOA (Chhabra et al., 2010). The fragments at m/z 43 (mainly $C_2H_3O^+$) and m/z 44 (mainly CO_2^+) can help retrieving information about ageing and oxidation state of secondary organic aerosol (SOA) (Ng et al., 2010, 2011a).

The four fragments mentioned above are shown in Fig. 2b as fraction of the total organic signal for all 15 participating instruments during the 20 h period mentioned above. As already represented in the colour bar of Fig. 2a it is evident that while most fragments have more or less similar contributions to total organic matter (e.g. f_{29}, f_{43} and f_{60} in Fig. 2b), there is significant instrument-to-instrument variation of the f_{44}. It is to note that the organic signals at m/z 16, 17 and 18 are also calculated from m/z 44 according to the fragmentation patterns highlighting the importance of the f_{44} variations (see Fig. 2a). A comparison of the mass spectra after the stick at m/z 44 and all related peaks were removed shows very similar relative spectra (IQR/median $< 20\,\%$ for most m/z, see Fig. S2 in the Supplement). Only m/z 29 which is mostly CHO^+ still shows a small increase (see Fig. S2b). This may either indicate a connection to m/z 44 (CO_2^+) or a small influence of air interferences.

Figure 2c shows that estimated O : C ratios based on f_{44} (Aiken et al., 2008) in this study varied from 0.41 to 0.77 for the same ambient aerosol. An elemental analysis of the HR-AMS data however yielded an O : C ratio of 0.38. This is close to the O : C ratio calculated from the formula of Aiken et al. (2008) for the HR-AMS spectrum (0.42). The consistency of the HR-AMS elemental analysis was confirmed by comparison to a known organic mixture beforehand. As a consequence the "real" O : C value during the intercomparison campaign most likely lies at the low end of Fig. 2c and the ACSMs overestimate O : C.

The fraction of m/z 44 to total organic matter measured (f_{44}) continuously varies compared to the mean between factors of 0.6 and 1.3 (from 8.5 and 18.2 %, Fig. 2b). Although the absolute value of f_{44} that is measured by different instruments is variable, all the instruments measure similar trends for f_{44}. The ratio of f_{44} between the instruments with even the highest and lowest f_{44} values, for example, is generally constant over time and does not vary with aerosol composition (see Fig. S3). Moreover, the precision of an individual, stable instrument is good and relative changes observed for any given instrument can be unambiguously interpreted. Thus, source apportionment analyses are not compromised, and indeed are only slightly affected as discussed hereafter.

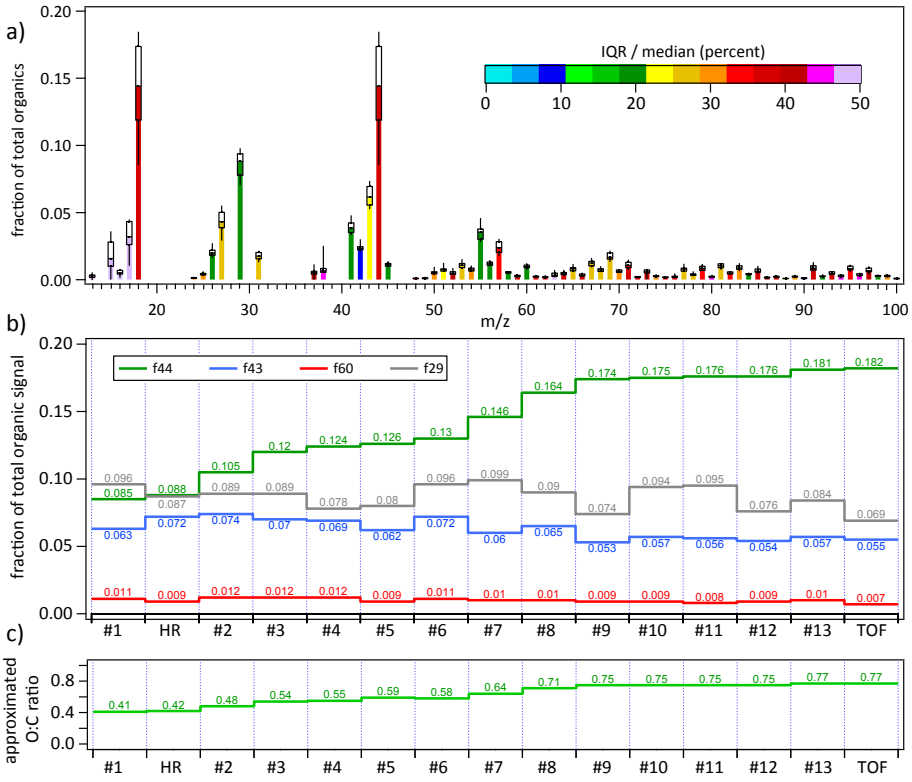

Figure 2. (a) Median organic mass spectrum of the 13 Q-ACSMs (sticks) during interruption-free 20 h period (average of ∼ 1200 mass spectra). The boxes represent the interquartile range for each m/z stick and the whiskers represent the corresponding full range over all instruments. The line in the box indicates the median. The colour bar represents the ratio of the width of the individual boxes in relation to the corresponding median in percent. **(b)** Fractions of the total organic signal at single m/z channels for all 15 participating instruments sorted by fraction of m/z 44. Grey: f_{29}, blue: f_{43}, green: f_{44}, red: f_{60}. The respective fractions are given as numbers in the same colours. **(c)** O : C ratio calculated via the formula given in Aiken et al. (2008) for all 15 participating instruments sorted by f_{44}. O : C values are also given as numbers.

Measurements of organic standards could be used to calibrate and allow for the intercomparison of the absolute f_{44} values observed in different ACSM instruments. However, in the absence of these calibrations, caution should be exercised in quantitatively comparing f_{44} values obtained by different ACSM instruments. This includes application of the f_{44} vs. f_{43} "triangle plot" (Ng et al., 2010) that is widely used to describe oxygenated organic aerosol (OOA) factors and comparisons of O : C values derived from ACSM f_{44} values.

A direct influence of the vaporiser temperature on this variability is deemed unlikely by ACSM measurements of several ambient aerosols (nebulisation of filter extracts, see Daellenbach et al., 2015, for method description) at different vaporiser temperatures. Relative organic spectra remained constant over a wide range of temperatures (see Fig. S4 and caption) as was already shown for several organic standards by Canagaratna et al. (2015). Also the fragmentation of inorganic molecules remained constant over a range of at least $550 \pm 70\,^{\circ}\mathrm{C}$.

The f_{44} variability is observed to be larger in the ACSM instruments than the AMS instruments (Ng et al., 2011c; Canagaratna et al., 2007). The ACSM and AMS instruments are based on the same particle vaporisation and ionisation schemes (using the identical particle vaporiser), but they are operated with different open/closed or open/filter switching cycles required for background subtraction. AMS instruments are typically operated with a faster switching cycle (< 5 s) than the Q-ACSMs (∼ 30 s), which in turn have shorter open times than the ToF-ACSM with the "fast-mode MS" setting (Kimmel et al., 2011) employed in this campaign (480 s open/120 s closed). It is noted that a fast filter switching scheme analogous to that of the Q-ACSM has now been implemented for the ToF-ACSM. The different switching times may result in different degrees of sensitivity to delayed vaporisation and pyrolysis artefacts. Efforts to understand and diminish the variability in f_{44} measured by ACSM instruments are ongoing.

3.3 HR-ToF-AMS source apportionment

Several publications have demonstrated that higher time and m/z resolution provided by the HR-ToF-AMS in contrast to

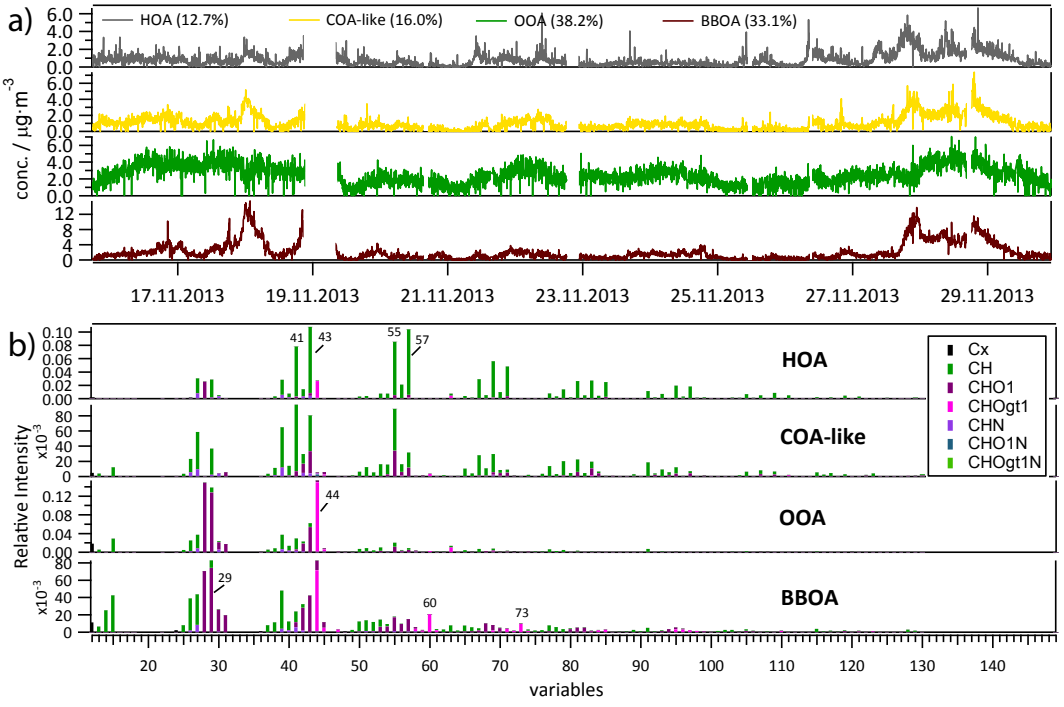

Figure 3. Factor time series in µg m^{-3} **(a)** and relative factor profiles **(b)** of the HR PMF source apportionment. In both (**a** and **b**) the factors are ordered from top to down as follows: HOA (grey), COA-like (yellow), OOA (green), BBOA (brown). Average contributions of each factor are given in brackets in **(a)**. The profiles are shown on a UMR axis with different colours for the various species families (see legend in the plot, gt here means "greater than").

the UMR of the ACSM result in less rotational ambiguity and provide superior source resolution (Aiken et al., 2009; Zhang et al., 2011). Therefore, we first performed a PMF of the HR-ToF-AMS data to determine the likely resolvable factors and their characteristics. High-resolution analysis was performed up to a mass-to-charge ratio of 130 resulting in 355 different organic fragments.

Completely unconstrained PMF analysis yielded four factors: hydrocarbon-like organic aerosol (HOA), cooking-like organic aerosol (COA), oxygenated organic aerosol (OOA) and biomass burning related aerosol (BBOA). Higher numbers of factors resulted in random splitting of already identified factors. However, in the four-factor solution, the HOA and COA factors showed signs of source mixing (mainly with the wood burning related source) like covariance of several factors. An extension of the analysis up to eight factors led to an unmixing of the two factors. Therefore, these clearly resolved HOA and COA factor profiles from the eight-factor solution were extracted, saved and used as anchors in a subsequent four-factor ME-2 analysis with tight constraints of $a = 0.1$ each. The other two factors remained unconstrained. This approach resulted in better correlations with external tracers for all factors than the completely unconstrained four-factor solution. A similar approach of increasing the number of factors in unconstrained PMF and subsequent combination of duplicate factors was used in previous studies (Docherty et al., 2011; Li et al., 2014). The resulting time series and factor profiles are shown in Fig. 3a and b. For more details about the PMF analysis of the HR data please refer to Sect. 3 of the Supplement.

Factors 1, 2 and 4 are attributed to POA sources while factor 3 is attributed to SOA. The identification of the factor sources is supported by correlations of profiles to known source spectra, by correlation to time series of the externally measured tracers explained below (see Fig. S5a–d and Table S4) and by identification of diurnal emission patterns (see Fig. 4).

Factor #1 (HOA) is dominated by ions related to aliphatic hydrocarbons, e.g. at m/z 41 ($C_3H_5^+$), m/z 43 ($C_3H_7^+$), m/z 55 ($C_4H_7^+$), m/z 57 ($C_4H_9^+$), m/z 67 ($C_5H_7^+$), m/z 69 ($C_5H_9^+$), m/z 71 ($C_5H_{11}^+$), m/z 79 ($C_6H_7^+$), m/z 81 ($C_6H_9^+$) and m/z 83 ($C_6H_{11}^+$) (Zhang et al., 2005b). HOA typically is emitted by combustion engines, e.g. from motor vehicles and believed to mainly come from lubricating oils (Canagaratna et al., 2004). The diurnal variation (Fig. 4) shows two clear peaks during morning and evening rush hours and the time series correlates well with ambient NO_x ($R^2 = 0.65$) concentrations and fossil fuel-related fraction of BC_{ff} retrieved from the Aethalometer ($R^2 = 0.68$).

The mass spectrum of factor #2, identified as organic aerosol related to cooking activities, shows similarities to the HOA with highest contributions of peaks at similar mass-to-

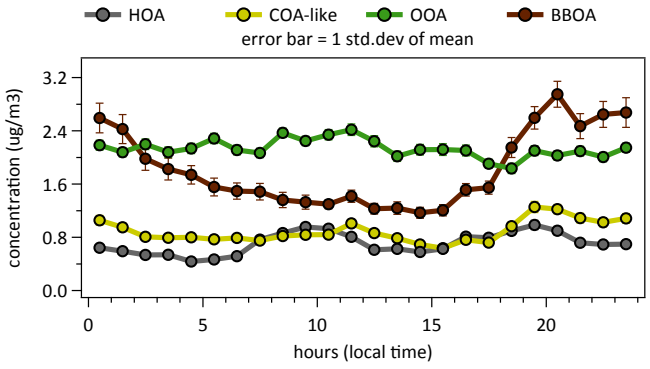

Figure 4. Diurnal variation (local time) of absolute factor concentrations in $\mu g\,m^{-3}$ (CE = 0.5, $RIE_{org} = 1.4$). Grey: HOA, yellow: COA-like, green: OOA, brown: BBOA. The error bars represent the first standard deviation (SD). In some cases (e.g. HOA) the error bars are not visible because they are smaller than the marker size.

charge ratios (m/z 27, 41, 43, 55, 57, 67, 69, 79, 81, 83) but with a higher contribution of oxygenated species at m/z 41 (C_2HO^+), m/z 43 ($C_2H_3O^+$), m/z 55 ($C_3H_3O^+$), m/z 57 ($C_3H_5O^+$), m/z 69 ($C_4H_5O^+$), m/z 71 ($C_4H_7O^+$), m/z 81 ($C_5H_5O^+$) and m/z 83 ($C_5H_7O^+$). This is in accordance with previous publications (Slowik et al., 2010; Allan et al., 2010; Mohr et al., 2012; Canonaco et al., 2013; Crippa et al., 2013a, 2014). Especially the oxygenated fragment at m/z 55 can serve as a good indicator for COA. $C_3H_3O^+$ is plotted together with the COA factor in Fig. S5b. Its correlation to COA ($R^2 = 0.80$) is much higher than to HOA ($R^2 = 0.38$). Also $C_6H_{10}O^+$ which was identified as a marker for COA before by Sun et al. (2011) and Crippa et al. (2013b) correlates better with the COA factor ($R^2 = 0.38$) than with the HOA factor ($R^2 = 0.23$, see grey trace in Fig. S5b). Typical for COA aerosol are the distinctively different (compared to the HOA factor) ratios between m/z 41 and 43, between m/z 55 and 57 and between m/z 69 and 71 (Mohr et al., 2012; Crippa et al., 2013a). In Fig. S6 the COA factor mass spectrum from this study is plotted side-by-side with the COA factor identified at the same station close to Paris in summer 2009. To date no reliable external tracer number for COA was established but the clear emission peaks during lunch and dinner time in the diurnal variation (Fig. 4) are characteristic of clearly resolved COA factors in previous studies and support the present interpretation.

The secondary factor #3 consists of highly oxidised (high f_{44}) organic aerosol (OOA). The diurnal cycle is more or less flat and the overall concentrations are more driven by meteorology than by emissions (see OOA time trace in Fig. 3a). This is supported by the stronger correlation of OOA to sulfate ($R^2 = 0.43$), ammonium ($R^2 = 0.54$), and nitrate ($R^2 = 0.47$, see Fig. S5d) than for the other three factors (see Table S4). As is frequently the case for winter campaigns, the OOA could not be further separated into oxygenation/volatility-dependent fractions (Lanz et al., 2010; Zhang et al., 2011).

The most descriptive features in the mass spectrum of factor #4 identifying it as BBOA are the oxygenated peaks at m/z 60 ($C_2H_4O_2^+$) and m/z 73 ($C_3H_5O_2^+$). They are associated with fragmentation of levoglucosan and other anhydrous sugars which are produced in the devolatilisation of cellulose making it a good tracer for biomass burning emissions (Simoneit et al., 1999; Hu et al., 2013a). Generally BBOA profiles from different measurement sites are less uniform than e.g. HOA profiles because of the higher variability of fuel and burning conditions (Weimer et al., 2008; Grieshop et al., 2009; Heringa et al., 2011, 2012; Crippa et al., 2014). The BBOA factor profiles from this study contain relatively high f_{44} which may be an indication of ageing and oxidation prior to detection but variations of the BBOA profile can also occur at the source (Young et al., 2015). Similar BBOA spectra were observed before, e.g. in winter in Paris (Crippa et al., 2013a) and in Zurich (Canonaco et al., 2013). The diurnal variation shows a steep increase in the afternoon and evening and a subsequent decrease after midnight, corresponding with domestic heating habits. In Fig. S5c the BBOA factor shows very good correlation with BC_{wb} from the Aethalometer ($R^2 = 0.90$) and to gas-phase methanol ($R^2 = 0.76$) and a reasonable correlation with acetonitrile ($R^2 = 0.48$) measured with a PTR-MS. In winter wood combustion is a significant source for primary and secondary methanol (Holzinger et al., 1999; Jacob et al., 2005; Gaeggeler et al., 2008; Akagi et al., 2013).

Overall factor contributions in the analysis of the HR-ToF-AMS data are: HOA 12.7 %, COA 16.0 %, OOA 38.2 %, BBOA 33.1 %. Relative contributions, number and type of factors as well as the fingerprint of factor profiles are in good agreement with results of Crippa et al. (2013a) from winter 2010 at a nearby site.

The amount of factors (four) found in this HR-PMF analysis provides the basis for the analysis of the parallel unit mass resolution (UMR) data sets from the further 13 Q-ACSMs and the 1 ToF-ACSM. The resolving power of the ToF-ACSM is sufficient to resolve a subset of the ions used in the HR-PMF analysis described here (Fröhlich et al., 2013). However, the uncertainties associated for inclusion in an HR-PMF study using the ToF-ACSM data are still undetermined. Therefore only UMR analyses of the ToF-ACSM data were performed for this intercomparison study.

3.4 ACSM (UMR) source apportionment

PMF analyses were performed individually on all 14 ACSM data sets. The data preparation procedures were described in Sect. 2.5 and Table S3. For most instruments, an unconstrained PMF analysis (no additional constraints on any of the factor profiles) could only resolve three separate factors (HOA, BBOA, OOA). The three-factor solutions showed larger instrument-to-instrument variability and less correla-

tion to external measurements for most ACSMs (especially of the HOA factor) than the four-factor ME-2 solutions presented hereafter. Amongst others, these points present a strong argument against the three-factor unconstrained PMF and for an introduction of a COA profile also if the additional information of the HR-AMS PMF was not available in the first place. Contributions and correlations of the three-factor PMF can be found in Fig. S7 and Table S5.

It is noted that although four factors could not be separated by an unconstrained PMF of the ACSM data, several indicators (increased seed variability, residuals of m/z 55, etc.) provide motivation for an extension of the analysis to higher factor numbers using the additional methods implemented in ME-2 to investigate the solution space outside the global minimum of Q (e.g. with profile constraints). In other words, also without the information of the HR PMF it is apparent that the three-factor PMF is not the best possible solution for the ACSMs.

Based on the HR-PMF analysis presented in Sect. 3.3 a COA factor was introduced with a variable a value. A verified anchor spectrum from a previous study at the nearby measurement site SIRTA zone 1 of Crippa et al. (2013a) was used (reference spectra from Crippa et al. (2013a) are labelled with the subscript Paris in the following). The HOA factor, if possible, remained unconstrained or was extracted from a previous PMF solution with a higher number of factors similar to the retrieval of the COA factor in the HR-PMF in Sect. 3.3. This procedure was favoured because for most ACSM an increase of the factor number produced an HOA factor with similar or better covariance with the time series of NO_x and BC_{ff} as opposed to the application of external reference HOA spectra. For this purpose unconstrained PMF runs with three, four, five and six factors were performed for each ACSM and the HOA profiles corresponding to the highest combined R^2 between factor time series and external data were saved and subsequently used as anchor profiles in the four-factor constrained ME-2 runs. HOA reference profiles retrieved this way are individual for each instrument and denoted HOA_{indv} in the following. A COA factor could not be extracted for the ACSM with this method. The HOA factors in the four-factor constrained ME-2 runs were left unconstrained if their time series correlations with NO_x and BC_{ff} were better or similar to the constrained case. The two additional factors in the 4 factor constrained ME-2 were left completely free and the results resembled OOA and BBOA for each instrument. Extraction of individual reference profiles directly from the data is not always possible and a more common approach is the adaptation of reference spectra from a database of previous experiments. Therefore the ME-2 results acquired with the use of the database profiles HOA_{Paris} and COA_{Paris} are shown as well for comparison. The influence of an alternative anchor (see Fig. 7, top panel, and Sect. 3.5.3) proved to be small for most ACSMs. However, there are outliers with larger differences in the factor contributions (e.g. #7, #12, TOF) which indicates that by testing a set of reference profiles, if possible, an improvement of the individual source apportionment can be reached. The source apportionment of the ToF-ACSM data produces clearer diurnal trends due to less scatter in the time series and higher temporal resolution compared to the Q-ACSM data. This facilitates source identification. In this study, however, for a clear separation of all four factors without the extra information of HR fitted spectra, the additional controls (e.g. possibility to introduce anchor spectra) of the ME-2 package were necessary for the source apportionment of both, ToF-ACSM and Q-ACSM data. Details about procedures for the selection of optimal a values can be found in Sect. 2.6.

Table 2. a values of the best solutions for each instrument. Anchors used in the ME-2 analysis: HOA anchor left table column: individual reference spectra from previous unconstrained PMF solution of the same data set (HOA_{indv}), right table column: HOA_{Paris}, COA anchors left and right table columns: COA_{Paris}. In some cases (#2, 3, 4 and 12) the time series correlation with external tracers was better (higher R^2) without constraint of the HOA profile.

a value	HOA_{indv} / COA_{Paris}	HOA_{Paris} / COA_{Paris}
ToF	0.05/0.05	0.10/0.10
#1	0.05/0.05	0.35/0.05
#2	free/0.04	0.25/0.15
#3	free/0.10	0.20/0.10
#4	free/0.15	0.15/0.15
#5	0.05/0.15	0.45/0.25
#6	0.05/0.05	0.30/0.30
#7	0.05/0.05	0.05/0.25
#8	0.05/0.05	0.20/0.15
#9	0.10/0.10	0.35/0.05
#10	0.04/0.20	0.20/0.20
#11	0.01/0.04	0.10/0.05
#12	free/0.10	0.20/0.30
#13	0.05/0.05	0.60/0.05

Optimised a values for each instrument are shown in Table 2. In some cases no clear maximum of the temporal correlation to external tracers but a plateau of the correlation coefficient R^2 could be found and the largest possible a value is noted in Table 2. This indicates a stable HOA factor. The COA factor which could not be resolved in the unconstrained PMF of the ACSM data sets is less stable and therefore generally needs a tighter constraint, i.e. a lower a value (see right column of Table 2). This is necessary to avoid as much as possible potential mixing of COA and BBOA factors. Similar diurnal cycles of heating and cooking activities (both sources have the highest emissions during the evening hours) pose a risk for factor mixing especially in the Q-ACSM data sets which have lower mass resolution and generally less precision. Two weeks of Q-ACSM measurement result in about 700 mass spectra of which only ~ 30 are including lunchtime COA emissions and the emission peak of COA aerosol in the evening overlaps with wood burning emissions. In addition

COA emissions may be significantly lower and partly transported in contrast to measurements at an urban site. All this may put COA at the edge of ME-2 resolvability. Due to this the Q-ACSM COA factor may still contain some mixed-in BBOA fraction or the other way round. Also the fact that the contribution of the COA factor stays well above zero during the night can be an indicator of some remaining factor mixing which cannot be resolved by ME-2 for this data set, of additional sources emitting COA-like aerosol more permanently like food industry or of regional transport or of the lower mixing height of the planetary boundary layer during night. Due to the first two points, real COA emissions may be somewhat lower than indicated by the COA factor and the factor is named COA-like in the following. For HOA_{indv} a smaller range of a values ($a = 0.01$–0.10; $\Delta a = 0.01$) was explored to maintain similarity to the extracted profiles.

3.5 Intercomparison of source apportionment results

3.5.1 Time series

Diurnal variation and factor profiles of all 15 solutions ($13 \times$ Q-ACSM, $1 \times$ ToF-ACSM, $1 \times$ HR-ToF-AMS) are displayed in Fig. 5 (for full time series see Fig. S9) and Figs. S15 and S16. To avoid influence of a potentially varying CE, the diurnal plots show the relative fractions of the total apportioned organic matter for the respective source factors instead of absolute concentrations. The diurnal variation plots of the four factors show the median of all Q-ACSMs (black) and the IQR as well as the 10–90 percentile range together with the diurnal variation of AMS (pink) and ToF-ACSM (green) factors. To facilitate comparison and to avoid a too large influence of the drift observed in the ToF-ACSM (see Sect. 2.5), all diurnal time traces (Q-ACSMs, HR-ToF-AMS and ToF-ACSM) were calculated only for the measurement period between 20 November and 2 December, discarding the first 4 days of measurement in which the observed exponentially decaying drift had the largest influence. Morning and evening rush hour peaks in the HOA as well as lunch and dinner time peaks in the COA-like factor are easily discernible around 1 p.m. and 9 p.m. The fraction of BBOA significantly increases in the evening when domestic heating activities are highest and decreases again after midnight with a small plateau in the morning when people are waking up. The apparent decrease of the OOA relative contribution in the evening can be attributed to the increase of BBOA since the absolute concentrations of OOA show no diurnal trends (see Fig. S9). The observed trend of the diurnal variations are similar in all 15 instruments. The full time series of all devices normalised to the total concentration measured with the HR-ToF-AMS are shown in Fig. S9. Correlations of these normalised factor time series to the median of all instruments are illustrated in the Supplement in Figs. S10–S13. Slopes range between 0.73–1.27 (HOA), 0.62–1.43 (COA-like), 0.77–1.23 (BBOA) and 0.66–1.28 (OOA) with correlation coefficients R^2 between 0.63–0.94 (HOA, median R^2: 0.91), 0.55–0.91 (COA-like, median R^2: 0.85), 0.90–0.98 (BBOA, median R^2: 0.95) and 0.72–0.95 (OOA, median R^2: 0.91).

Diurnal variation of the relative factor contributions from the HR-AMS and the ToF-ACSM data sets are largely within the range of the Q-ACSMs. The morning peak of the HOA is slightly smaller in the HR-AMS than in the other devices (morning traffic peak contributions: 22.5 % (HR-AMS), 27.7 % (median Q-ACSMs), 30.4 % (ToF-ACSM)) and the source apportionment of the ToF-ACSM data set yielded slightly lower OOA but higher BBOA concentrations (see Fig. 7, bottom panel). It is noted that the non-uniform time steps the Q-ACSM data are recorded at, and several unplanned measurement interruptions of some of the instruments, made it impossible to completely synchronise all devices. This contributes an unknown, likely small fraction of the total uncertainty.

The lower panel of Fig. 5 shows the diurnal variation of the model residuals scaled to the total organic concentrations. Residuals of ToF-ACSM and Q-ACSMs fluctuate around zero and are always within a range smaller than ± 2 % of total organic concentrations. In the evening hours when total organic concentrations are highest the scaled residuals tend to be slightly larger. The HR-AMS residuals, however, are higher and purely positive. A more detailed analysis shows that all m/z channels are affected to a similar extent. The reason for the purely positive residuals is unknown, but no significant temporal variation and no significant change or decrease of the residuals even in PMF runs with high number of factors (> 10) indicate that the residuals are not connected with additional factors missing in the current analysis.

3.5.2 Profiles

The median factor profiles of the HOA, COA-like, BBOA and OOA factors of the 13 Q-ACSMs are shown as sticks in Fig. 6. IQR of each individual stick is displayed as a box while the full range is shown with the whiskers. Colours denote the width of the IQR box relative to the median. For the BBOA and OOA factors the m/z range between 50 and 100 is enlarged in separate insets. The typical features of each factor are similar to the HR data in Sect. 3.3.

The aliphatic hydrocarbon signals characteristic for HOA have relatively stable contributions to the HOA source spectrum (box $\lessapprox 15$ %, green colour) in all instruments. The variation of m/z 43 is slightly higher (≈ 25 %, yellow) and the mass-to-charge ratios 29 and 44 (and 16–18 which are calculated directly from m/z 44, see Allan et al., 2004) have quite large boxes (> 50 %, violet). These fragments are also partly apportioned to BBOA and OOA which could indicate a minor mixing of these sources into the HOA factor for some instruments. Considering the full range (whiskers), instrument #13 (see Fig. S15, also #1 and #5 show slightly elevated f_{44}) represents an outlier with high m/z 44 in the HOA. It is noted that in most ME-2 source apportionments this solution would

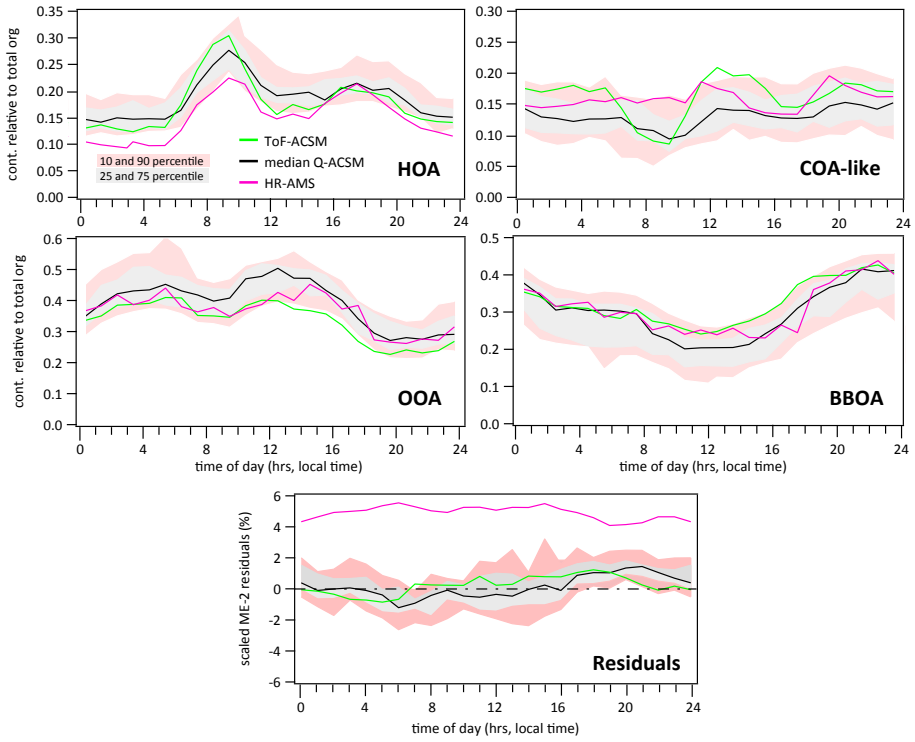

Figure 5. Diurnal variation of the four source factors and PMF residuals. The upper four panels display the relative contribution of the respective sources to the total apportioned organic matter. Top left: HOA, top right: COA-like, bottom left: OOA, bottom right: BBOA. Green trace: ToF-ACSM, pink trace: HR-ToF-AMS, black trace: median of all 13 Q-ACSMs. The IQR and the 10–90 percentile range of the Q-ACSMs are indicated as light grey and light red regions, respectively. The lower panel shows the residual organic concentration not explained by the presented solution in % of the total organic concentration. The time is local time (UTC+1 h). Hourly averages are displayed according to their time center (e.g. the data point at 12:30 represents the average between 12:00 and 13:00).

have been discarded and an approach with a constrained externally measured HOA profile would have been favoured (similar to the approach used to calculate the second bars from the left in Fig. 7, top panel). For the sake of comparability the solution with the individually extracted HOA profile of instrument #13 is still included in this analysis. Other contributing m/z channels which exhibit a larger variability of more than 30 % in the HOA profiles are 26, 27, 53, 66, 77 and 91.

The second panel of Fig. 6 shows the variation of the COA source profiles which were constrained with low a values. It is noted that the method of adding constraints to the ME-2 output naturally has an effect on its maximum possible variability. Therefore no variations $\gtrapprox 20$ % are observed.

The BBOA profile is shown in the third panel. The variations of the important markers at m/z 29, 60 and 73 show the smallest variations ($\lessapprox 25$ %). The f_{44} however exhibits a variability of ≈ 50 %. A more detailed look at the BBOA profiles in Fig. S16 shows a dependency on total f_{44}. While instruments with lower total f_{44} mostly have a lower f_{44} in the BBOA spectrum, devices with higher f_{44} on the other hand also tend to have higher f_{44} in their BBOA spectrum. This should be kept in mind for the application of f_{44} to characterise ageing of biomass burning plumes (as could be shown for AMS data by Cubison et al., 2011) from ACSM data sets.

The OOA factor profile shows only slightly smaller absolute variation (size of box) of f_{44} than the BBOA profile, but since here f_{44} is larger in general, the resulting size of the box in relation to the median is only of the order of ≈ 20 %. Considering the full range, f_{44} varies by about 40 %, similar to the variation of f_{44} in the input organic mass spectra. Again, a look at Fig. S16 reveals an increasing f_{44} in the OOA source profile with increasing total f_{44}. There are only a few additional m/z channels having significant contributions to OOA. The magnification of the region above m/z 50 shows only very low signals with high variations which predominantly can be considered noise.

The fact that the f_{44} has a high instrument-to-instrument variability in all unconstrained factors has important implications for the application of reference profiles measured with an AMS or another ACSM to ACSM data sets. Constraints on m/z 44 should be avoided or loosened as much as possible. Alternatively the f_{44} in such reference profiles should be subjected to a sensitivity test (e.g. by manually changing the f_{44} of a reference profile).

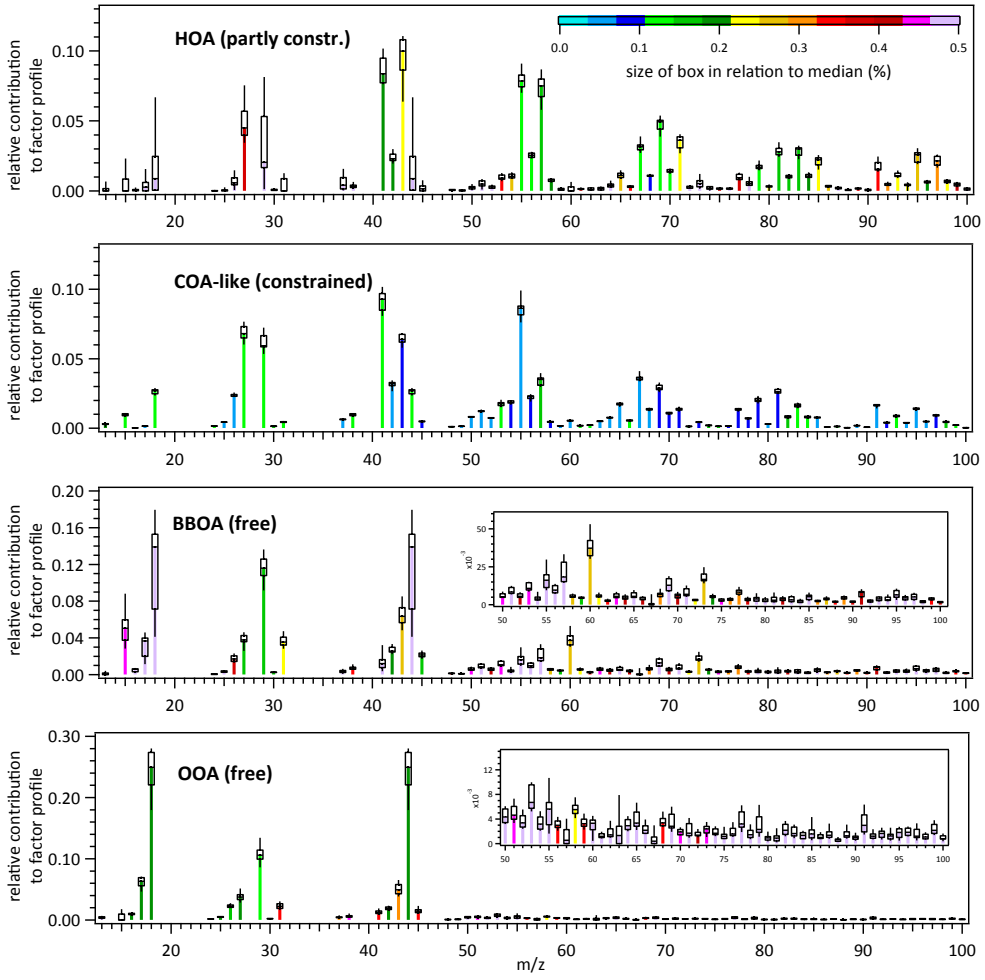

Figure 6. Median source factor profiles of the 13 Q-ACSMs (sticks) sorted from top to bottom as follows: HOA, COA-like, BBOA, OOA. The boxes represent the IQR for each m/z stick and the whiskers represent the corresponding full range over all instruments. The line in the box indicates the median. The colour bar represents the ratio of the width of the individual boxes in relation to the corresponding median in percent. The region between m/z 50 and 100 is enlarged in the two small insets for the BBOA and the OOA factor.

The source profiles of the ME-2 analysis of the ToF-ACSM data set are shown in Fig. S14 together with box and whisker plots of the Q-ACSM profiles. Generally the ToF-ACSM source profiles lie well within the range of the Q-ACSMs. Since the ToF-ACSM had the highest f_{44} of all instruments all factor profiles lie at the upper end of the Q-ACSM f_{44} range. The signals at higher mass-to-charge ratios are a bit smaller. This could either be due to an overestimation of the RIT correction performed on the Q-ACSM mass spectral data (see RIT discussion in the Supplement) or to loss of smaller signals in the ToF-ACSM caused by the operational issue with the detector amplification detailed in Sect. 2.5. The latter is unlikely but cannot be completely excluded.

3.5.3 Contributions

For the comparison of ME-2 SA performance on ACSM data one of the important variables are the source contributions. In Fig. 7 (top panel) the respective source contributions of all participating instruments are plotted as bar plots for four different solutions. From left to right the bars stand for:

- ME-2 solution with constrained $\mathrm{COA_{Paris}}$ and (if necessary, see Table 2) $\mathrm{HOA_{indv}}$; a values optimised.
- ME-2 solution with constrained $\mathrm{COA_{Paris}}$ and $\mathrm{HOA_{Paris}}$; a values optimised according to description in Sect. 3.4.
- ME-2 solution with constrained $\mathrm{COA_{Paris}}$ and $\mathrm{HOA_{Paris}}$; a_{COA} as above but a_{HOA} completely fixed ($a_{\mathrm{HOA}} = 0$).
- ME-2 solution with constrained $\mathrm{COA_{Paris}}$ and $\mathrm{HOA_{Avg}}$; a_{COA} as above but a_{HOA} completely fixed ($a_{\mathrm{HOA}} = 0$).

HOA_{Avg} represents the average of 15 ambient HOA profiles (Ng et al., 2011b).

The HR case on the left of Fig. 7 is an exception. There only the solution presented in Sect. 3.3 is shown because the UMR profiles HOA_{Paris} and HOA_{Avg} cannot be used for HR data and the ion list of the HR COA profile from Crippa et al. (2013a) did not fully overlap with our ion list.

HOA_{Paris} and HOA_{Avg} are relatively similar to each other. Due to this, in some instruments even with fixed HOA anchors the resulting contributions are very similar (e.g. #1, #8 and #13) while for others (e.g. #3, #12 and ToF) the contributions of the fixed case differ significantly, nonetheless. As a consequence a sensitivity test of a wide range of a values is always recommended. By relaxing the constraints (i.e. increasing/optimising the a value) the ME-2 results of different instruments tend more towards similar solutions. A comparison of the two fully coloured bars of each instrument in most cases reveals only minor differences in the relative source contributions to total organic matter measured (largest deviations at #1–3 and #5–7), leading to the assumption that the choice of reference HOA spectrum is not too crucial if the a values are optimised.

Median and average contributions of each of the four factors are summarised in Table 3 together with the corresponding SDs. HOA contributed 14.3 ± 2.2 %, COA 15.0 ± 3.4 %, OOA 41.5 ± 5.7 % and BBOA 29.3 ± 5.0 % to the total organic mass. It is noted that average concentrations over the 15-day period were $6.9\,\mu g\,m^{-3}$ (range ≈ 0.7–$25\,\mu g\,m^{-3}$, see Fig. 1) and higher or lower signal-to-noise ratios or differences in the source time series variability have an effect on the accuracy of the results. Usually lower average concentrations or less temporal variability will increase the uncertainties while higher average concentrations or increased temporal variability will decrease the uncertainties. The uncertainties found in this study are shown in more detail in Fig. 7 (bottom panel). There the individual deviations of all factors from the median are shown in percent for all participating instruments. The ± 15 % region is indicated by the dashed line and the ± 30 % region by the solid line. Most deviations lie within the ± 15 % region – in particular, HOA, OOA and BBOA have only few outliers (HOA: 3, BBOA: 4, OOA: 3), while COA-like factor has significantly more (7 outliers). This emphasises the already discussed notion that COA was the most difficult factor to quantify because of the temporally low occurrence (lunchtime) of significant events and its partial concurrence with the BBOA in the evening hours. Therefore COA also possesses the highest uncertainties in this study.

Over- and underestimation of all four factors appear more or less randomly distributed – no significant dependence on f_{44} is noticeable. This suggests that the differences in the input data matrix (see Sect. 3.2), mainly the f_{44}, do not contribute significantly to the relatively small discrepancies of the factor contributions between the 15 instruments (Table 3) even though source spectra can differ significantly between instruments (see Sect. 3.5.2). This indicates a correct allocation of the additional m/z 44 signal which may originate from pyrolysed organic compounds to the original aerosol source.

Table 3. Median and average factor contributions over all 15 participating instruments.

factor	median (%)	average (%)	SD (%)
HOA	14.7	14.3	2.2
COA-like	14.9	15.0	3.4
OOA	42.8	41.5	5.7
BBOA	29.2	29.3	5.0

Figure S17 shows the same results in terms of z score values (calculated in accordance with ISO13528, 2005), a dimensionless statistical quantity (see Eq. S1) evaluating the performance of each source apportionment solution with respect to a reference value using the robust standard deviation of the contributions as target uncertainty (Karagulian and Belis, 2012; Belis et al., 2015). The same method was employed in part 1 of this study by Crenn et al. (2015). With two exceptions (HOA in instrument #13 and OOA in the ToF-ACSM) all results lie in the "ok" and "acceptable" regime defined by $|z| \leq 2$.

It is noted that the stated uncertainties are only the relative uncertainties of the source apportionment, not taking into account the additional variation of total measured organic mass between instruments, which is assessed in part 1 of this study (Crenn et al., 2015). Average concentrations and first SD in $\mu g\,m^{-3}$ of each source are given in Table S6, representing the combination of both sources of uncertainty. Additionally it is noted that potential differences in CE of different OA sources, as was speculated e.g. by Yin et al. (2015), are not accounted for.

3.5.4 ACSM specific recommendations

Crippa et al. (2014) developed a standardised approach for ME-2 analyses of AMS measurements in addition to the recommendations given by Ulbrich et al. (2009). Since ACSM data is basically identical to UMR AMS data with reduced temporal resolution, a similar approach is recommended for ACSM data sets. Additionally, several ACSM-specific points are suggested by the current study:

– Profile constraints on the m/z 44 signal should be avoided or kept as loose as possible (high a value for m/z 44).

– If constraints are applied to the m/z 44 signal, a sensitivity analysis, e.g. by manual modification of the relative amount of the m/z 44 signal is recommended.

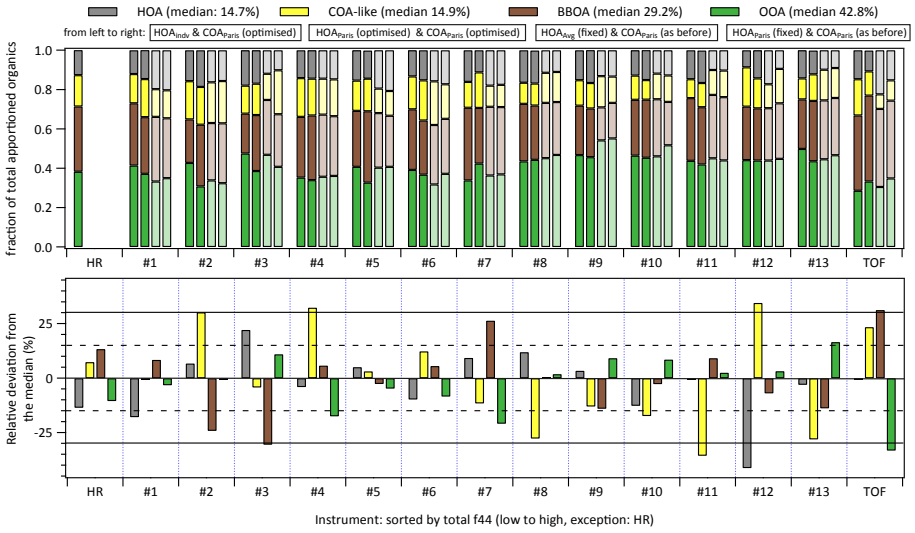

Figure 7. (Top) Relative factor contributions of HOA (grey), COA-like (yellow), OOA (green) and BBOA (brown) for each of the 15 participating instruments sorted by f_{44} in the corresponding total organic spectrum (low to high). Each time four bar plots are shown. Fully coloured: a values were optimised, lightly coloured: $a_{HOA} = 0$ and a_{COA} equal to value in the second fully coloured bar from the left (see Table 2). For each of the left-most bar plots HOA was either fully unconstrained or HOA_{indv} extracted from a previous unconstrained PMF solution of the same data set. For the second bar the anchors HOA_{Paris} and COA_{Paris} were used and optimised in each case. For the third and fourth bar from the left COA_{Paris} was used as anchor with the same a values as before while $a_{HOA} = 0$. Different HOA anchors were used in the third (HOA_{Avg}) and the fourth (HOA_{Paris}) bars from the left. Median values of the left-most solutions are given in brackets in the legend. (Bottom) Relative deviation from the median in percent of each factor in each of the 15 instruments sorted by total f_{44} (low to high). The solid line confines the ± 30 % region and the dashed line the ± 15 % region. Colours are the same as in the top panel.

– All Q-ACSM measured non-physical negative mass concentrations at mass-to-charge ratio 12. Therefore m/z 12 should be removed in PMF/ME-2 source apportionments of Q-ACSM data. To avoid negative m/z 12 in future data sets, the waiting time between quadrupole scans should be increased in the DAQ software.

– Anchor profiles constructed from the studied data set are preferable to database profiles. These profiles can often be extracted from solutions with additional factors (e.g. this study) or from separate PMF on parts of the data set with high fractional contributions of a factor (e.g. period with nearby forest fires or high primary traffic emissions).

– The PMF results of short-term, high-resolution AMS measurements overlapping with long-term ACSM measurements can provide useful constraints on the source apportionment of the ACSM data set (e.g. number of factors, special features in a profile).

– If no profiles can be extracted with the methods described above, it is advised to try and compare different database anchor profiles (e.g. by comparing SA results to external data or comparing changes in diurnal cycles). This is more crucial for factors for which the profiles typically show larger variations between sites (e.g. BBOA, see Ng et al., 2011b) as opposed to factors with more similar profiles (e.g. HOA, see Ng et al., 2011b).

4 Conclusions

The ACTRIS ACSM intercomparison taking place for about 3 weeks (end of November to December 2013) at the SIRTA site in Gif-sur-Yvette near Paris provided great insight into the comparability of ACSM instruments, especially in terms of mass concentrations (part 1 of this study), mass spectra and source apportionment. Future exercises of this kind are encouraged. In this study, factor analysis source apportionment was performed on the data sets of 15 co-located aerosol mass spectrum analysers ($13 \times$ Q-ACSM, $1 \times$ ToF-ACSM, $1 \times$ HR-ToF-AMS) operated in parallel. To minimise external influence, operation (e.g. same operator of all source apportionments, use of the same software versions) and instrumentation (e.g. same calibration equipment) were harmonised. In each case four specific factors were identified: HOA, COA-like, OOA and BBOA sources, having features consistent with previous AMS studies at a nearby site (Crippa et al., 2013a). A better separation of the input variables due to the high resolution of the HR-ToF-AMS allowed for the identification of all four factors with unconstrained PMF. For the ACSM UMR data sets (including the ToF-ACSM) the ME-2 approach, partly constraining the HOA and COA profiles, was employed. The strength of the constraint (a value)

was optimised by maximisation of the correlation (R^2) of the factor time series with external tracer measurements.

The fraction of organic mass occurring at m/z 44 (f_{44}) varied between factors of 0.6 and 1.3 compared to the mean across all instruments. Such differences should be considered in comparing estimated O : C ratios and retrieved factor profiles between ACSMs. The f_{44} discrepancies do have significant influence on resulting factor profiles of ME-2/PMF analyses but no significant influence on total factor contributions was noticed.

A good agreement of relative factor contributions over all 15 instruments was found. On average HOA contributed 14.3 ± 2.2 %, COA 15.0 ± 3.4 %, OOA 41.5 ± 5.7 % and BBOA 29.3 ± 5.0 %. The listed first SDs give a measure for the uncertainty of the ME-2 source apportionment related to the measurement technique. From these numbers a relative deviation from the mean combined over all factors of ± 17.2 % was calculated.

The Supplement related to this article is available online at doi:10.5194/amt-8-2555-2015-supplement.

Acknowledgements. This work was conducted in the frame of the ACTRIS programme (European Union Seventh Framework Programme (FP7/2007-2013), grant agreement no. 262254). The authors acknowledge the French Agency of Environment and Energy Management (ADEME grants 1262C0022 and 1262C0039), the CaPPA (Chemical and Physical Properties of the Atmosphere) project (ANR-10-LABX-005) funded by the French National Research Agency (ANR) through the PIA (Programme d'Investissement d'Avenir), the EU-FEDER CORSiCA, Eurostars E!4825 and KROP, financed by the Slovenian Ministry of Economic Development and Technology, and ChArMEx projects. J. G. Slowik acknowledges support from the Swiss National Science Foundation (SNSF) through the Ambizione programme (PZ00P2_131673). V. Crenn acknowledges the DIM R2DS programme for his postdoctoral grant. J. Ovadnevaite and C. D. O'Dowd acknowledge HEA-PRTLI4 and NUIG's Research Support Fund. CIEMAT contribution has been partially funded by CGL2011-16124-E, CGL2011-27020 and CGL2014-52877-R actions from the Spanish National R&D Programme, and AEROCLIMA (Fundacion Ramon Areces, CIVP16A1811). IDAEA CSIC was partially funded by the Spanish Ministry of Economy and Competitiveness and FEDER funds under the PRISMA (CGL2012-39623-C02-1) project.

Edited by: J. Schneider

References

Aiken, A. C., DeCarlo, P. F., Kroll, J. H., Worsnop, D. R., Huffman, J. A., Docherty, K. S., Ulbrich, I. M., Mohr, C., Kimmel, J. R., Sueper, D., Sun, Y., Zhang, Q., Trimborn, A., Northway, M., Ziemann, P. J., Canagaratna, M. R., Onasch, T. B., Alfarra, M. R., Prevot, A. S. H., Dommen, J., Duplissy, J., Metzger, A., Baltensperger, U., and Jimenez, J. L.: O/C and OM/OC ratios of primary, secondary, and ambient organic aerosols with high-resolution time-of-flight aerosol mass spectrometry, Environ. Sci. Technol., 42, 4478–4485, 2008.

Aiken, A. C., Salcedo, D., Cubison, M. J., Huffman, J. A., DeCarlo, P. F., Ulbrich, I. M., Docherty, K. S., Sueper, D., Kimmel, J. R., Worsnop, D. R., Trimborn, A., Northway, M., Stone, E. A., Schauer, J. J., Volkamer, R. M., Fortner, E., de Foy, B., Wang, J., Laskin, A., Shutthanandan, V., Zheng, J., Zhang, R., Gaffney, J., Marley, N. A., Paredes-Miranda, G., Arnott, W. P., Molina, L. T., Sosa, G., and Jimenez, J. L.: Mexico City aerosol analysis during MILAGRO using high resolution aerosol mass spectrometry at the urban supersite (T0) – Part 1: Fine particle composition and organic source apportionment, Atmos. Chem. Phys., 9, 6633–6653, doi:10.5194/acp-9-6633-2009, 2009.

Aiken, A. C., de Foy, B., Wiedinmyer, C., DeCarlo, P. F., Ulbrich, I. M., Wehrli, M. N., Szidat, S., Prevot, A. S. H., Noda, J., Wacker, L., Volkamer, R., Fortner, E., Wang, J., Laskin, A., Shutthanandan, V., Zheng, J., Zhang, R., Paredes-Miranda, G., Arnott, W. P., Molina, L. T., Sosa, G., Querol, X., and Jimenez, J. L.: Mexico city aerosol analysis during MILAGRO using high resolution aerosol mass spectrometry at the urban supersite (T0) – Part 2: Analysis of the biomass burning contribution and the non-fossil carbon fraction, Atmos. Chem. Phys., 10, 5315–5341, doi:10.5194/acp-10-5315-2010, 2010.

Akagi, S. K., Yokelson, R. J., Burling, I. R., Meinardi, S., Simpson, I., Blake, D. R., McMeeking, G. R., Sullivan, A., Lee, T., Kreidenweis, S., Urbanski, S., Reardon, J., Griffith, D. W. T., Johnson, T. J., and Weise, D. R.: Measurements of reactive trace gases and variable O_3 formation rates in some South Carolina biomass burning plumes, Atmos. Chem. Phys., 13, 1141–1165, doi:10.5194/acp-13-1141-2013, 2013.

Alfarra, M. R., Prevot, A. S. H., Szidat, S., Sandradewi, J., Weimer, S., Lanz, V. A., Schreiber, D., Mohr, M., and Baltensperger, U.: Identification of the mass spectral signature of organic aerosols from wood burning emissions, Environ. Sci. Technol., 41, 5770–5777, 2007.

Allan, J. D., Delia, A. E., Coe, H., Bower, K. N., Alfarra, M., Jimenez, J. L., Middlebrook, A. M., Drewnick, F., Onasch, T. B., Canagaratna, M. R., Jayne, J. T., and Worsnop, D. R.: A generalised method for the extraction of chemically resolved mass spectra from Aerodyne aerosol mass spectrometer data, J. Aerosol Sci., 35, 909–922, 2004.

Allan, J. D., Williams, P. I., Morgan, W. T., Martin, C. L., Flynn, M. J., Lee, J., Nemitz, E., Phillips, G. J., Gallagher, M. W., and Coe, H.: Contributions from transport, solid fuel burning and cooking to primary organic aerosols in two UK cities, Atmos. Chem. Phys., 10, 647–668, doi:10.5194/acp-10-647-2010, 2010.

Belis, C., Karagulian, F., Amato, F., Almeida, M., Argyropoulos, G., Artaxo, P., Beddows, D., Bernardoni, V., Bove, M., Carbone, S., Cesari, D., Contini, D., Cuccia, E., Diapouli, E., Eleftheriadis, K., Favez, O., El Haddad, I., Harrison, R., Hellebust, S., Jang, E., Jorquera, H., Kammermeier, T., Karl, M., Lucarelli, F., Mooibroek, D., Nava, S., Nøjgaard, J. K., Pandolfi, M., Perrone, M., Petit, J., Pietrodangelo, A., Pirovano, G., Pokorná, P., Prati, P., Prevot, A., Quass, U., Querol, X., C., S., Saraga, D., Sciare, J., Sfetsos, A., Valli, G., Vecchi, R., Vestenius, M., Yubero, E., and Hopke, P.: Assessment of source apportionment models perfor-

mance: the results of two European intercomparison exercises, Atmos. Environ., submitted, 2015.

Bond, T. C. and Bergstrom, R. W.: Light absorption by carbonaceous particles: An investigative review, Aerosol Sci. Technol., 40, 27–67, 2006.

Boucher, O., Randall, D., Artaxo, P., Bretherton, C., Feingold, G., Forster, P., Kerminen, V.-M., Kondo, Y., Liao, H., Lohmann, U., Rasch, P., Satheesh, S. K., Sherwood, S., Stevens, B., and Zhang, X. Y.: Clouds and Aerosols, in: Climate change 2013: The physical science basis, contribution of working group I to the fifth assessment report of the intergovernmental panel on climate change, edited by: Stocker, T., Qin, D., Plattner, G.-K., Tignor, M., Allen, S., Boschung, J., Nauels, A., Xia, Y., V., B., and Midgley, P. M., Cambridge University Press, Cambridge, UK and New York, NY, USA, 571–657, 2013.

Bressi, M., Sciare, J., Ghersi, V., Mihalopoulos, N., Petit, J.-E., Nicolas, J. B., Moukhtar, S., Rosso, A., Féron, A., Bonnaire, N., Poulakis, E., and Theodosi, C.: Sources and geographical origins of fine aerosols in Paris (France), Atmos. Chem. Phys., 14, 8813–8839, doi:10.5194/acp-14-8813-2014, 2014.

Brown, S. G., Lee, T., Norris, G. A., Roberts, P. T., Collett Jr., J. L., Paatero, P., and Worsnop, D. R.: Receptor modeling of near-roadway aerosol mass spectrometer data in Las Vegas, Nevada, with EPA PMF, Atmos. Chem. Phys., 12, 309–325, doi:10.5194/acp-12-309-2012, 2012.

Canagaratna, M., Jayne, J., Jimenez, J., Allan, J., Alfarra, M., Zhang, Q., Onasch, T., Drewnick, F., Coe, H., Middlebrook, A., Delia, A., Williams, L., Trimborn, A., Northway, M., DeCarlo, P., Kolb, C., Davidovits, P., and Worsnop, D.: Chemical and microphysical characterization of ambient aerosols with the aerodyne aerosol mass spectrometer, Mass Spectrom. Rev., 26, 185–222, 2007.

Canagaratna, M. R., Jayne, J. T., Ghertner, D. A., Herndon, S., Shi, Q., Jimenez, J. L., Silva, P. J., Williams, P., Lanni, T., Drewnick, F., Demerjian, K. L., Kolb, C. E., and Worsnop, D. R.: Chase studies of particulate emissions from in-use New York City vehicles, Aerosol Sci. Tech., 38, 555–573, 2004.

Canagaratna, M. R., Jimenez, J. L., Kroll, J. H., Chen, Q., Kessler, S. H., Massoli, P., Hildebrandt Ruiz, L., Fortner, E., Williams, L. R., Wilson, K. R., Surratt, J. D., Donahue, N. M., Jayne, J. T., and Worsnop, D. R.: Elemental ratio measurements of organic compounds using aerosol mass spectrometry: characterization, improved calibration, and implications, Atmos. Chem. Phys., 15, 253–272, doi:10.5194/acp-15-253-2015, 2015.

Canonaco, F., Crippa, M., Slowik, J. G., Baltensperger, U., and Prévôt, A. S. H.: SoFi, an IGOR-based interface for the efficient use of the generalized multilinear engine (ME-2) for the source apportionment: ME-2 application to aerosol mass spectrometer data, Atmos. Meas. Tech., 6, 3649–3661, doi:10.5194/amt-6-3649-2013, 2013.

Carslaw, K. S., Boucher, O., Spracklen, D. V., Mann, G. W., Rae, J. G. L., Woodward, S., and Kulmala, M.: A review of natural aerosol interactions and feedbacks within the Earth system, Atmos. Chem. Phys., 10, 1701–1737, doi:10.5194/acp-10-1701-2010, 2010.

Carslaw, K. S., Lee, L. A., Reddington, C. L., Pringle, K. J., Rap, A., Forster, P. M., Mann, G. W., Spracklen, D. V., Woodhouse, M. T., Regayre, L. A., and Pierce, J. R.: Large contribution of natural aerosols to uncertainty in indirect forcing, Nature, 503, 67–71, 2013.

Chhabra, P. S., Flagan, R. C., and Seinfeld, J. H.: Elemental analysis of chamber organic aerosol using an Aerodyne high-resolution aerosol mass spectrometer, Atmos. Chem. Phys., 10, 4111–4131, doi:10.5194/acp-10-4111-2010, 2010.

Cohen, A. J., Ross Anderson, H., Ostro, B., Pandey, K. D., Krzyzanowski, M., Kunzli, N., Gutschmidt, K., Pope, A., Romieu, I., Samet, J. M., and Smith, K.: The global burden of disease due to outdoor air pollution, J. Toxicol. Env. Heal. A, 68, 1301–1307, 2005.

Collaud Coen, M., Weingartner, E., Apituley, A., Ceburnis, D., Fierz-Schmidhauser, R., Flentje, H., Henzing, J. S., Jennings, S. G., Moerman, M., Petzold, A., Schmid, O., and Baltensperger, U.: Minimizing light absorption measurement artifacts of the Aethalometer: evaluation of five correction algorithms, Atmos. Meas. Tech., 3, 457–474, doi:10.5194/amt-3-457-2010, 2010.

Crenn, V., Sciare, J., Croteau, P. L., Favez, O., Verlhac, S., Belis, C. A., Fröhlich, R., Aas, W., Aijälä, M., Alastuey, A., Artiñano, B., Baisnée, D., Baltensperger, U., Bonnaire, N., Bressi, M., Canagaratna, M., Canonaco, F., Carbone, C., Cavalli, F., Coz, E., Cubison, M. J., Gietl, J. K., Green, D. C., Heikkinen, L., Lunder, C., Minguillón, M. C., Močnik, G., O'Dowd, C. D., Ovadnevaite, J., Petit, J.-E., Petralia, E., Poulain, L., Prévôt, A. S. H., Priestman, M., Riffault, V., Ripoll, A., Sarda-Estève, R., Slowik, J., Setyan, A., and Jayne, J. T.: ACTRIS ACSM Intercomparison: part I - Intercomparison of concentration and fragment results from 13 individual co-located aerosol chemical speciation monitors (ACSM), Atmos. Meas. Tech. Disc., submitted, 2015.

Crippa, M., DeCarlo, P. F., Slowik, J. G., Mohr, C., Heringa, M. F., Chirico, R., Poulain, L., Freutel, F., Sciare, J., Cozic, J., Di Marco, C. F., Elsasser, M., Nicolas, J. B., Marchand, N., Abidi, E., Wiedensohler, A., Drewnick, F., Schneider, J., Borrmann, S., Nemitz, E., Zimmermann, R., Jaffrezo, J.-L., Prévôt, A. S. H., and Baltensperger, U.: Wintertime aerosol chemical composition and source apportionment of the organic fraction in the metropolitan area of Paris, Atmos. Chem. Phys., 13, 961–981, doi:10.5194/acp-13-961-2013, 2013a.

Crippa, M., El Haddad, I., Slowik, J. G., DeCarlo, P. F., Mohr, C., Heringa, M. F., Chirico, R., Marchand, N., Sciare, J., Baltensperger, U., and Prévôt, A. S. H.: Identification of marine and continental aerosol sources in Paris using high resolution aerosol mass spectrometry, J. Geophys. Res.-Atmos., 118, 1950–1963, 2013b.

Crippa, M., Canonaco, F., Lanz, V. A., Äijälä, M., Allan, J. D., Carbone, S., Capes, G., Ceburnis, D., Dall'Osto, M., Day, D. A., DeCarlo, P. F., Ehn, M., Eriksson, A., Freney, E., Hildebrandt Ruiz, L., Hillamo, R., Jimenez, J. L., Junninen, H., Kiendler-Scharr, A., Kortelainen, A.-M., Kulmala, M., Laaksonen, A., Mensah, A. A., Mohr, C., Nemitz, E., O'Dowd, C., Ovadnevaite, J., Pandis, S. N., Petäjä, T., Poulain, L., Saarikoski, S., Sellegri, K., Swietlicki, E., Tiitta, P., Worsnop, D. R., Baltensperger, U., and Prévôt, A. S. H.: Organic aerosol components derived from 25 AMS data sets across Europe using a consistent ME-2 based source apportionment approach, Atmos. Chem. Phys., 14, 6159–6176, doi:10.5194/acp-14-6159-2014, 2014.

Cubison, M. J., Ortega, A. M., Hayes, P. L., Farmer, D. K., Day, D., Lechner, M. J., Brune, W. H., Apel, E., Diskin, G. S., Fisher, J. A., Fuelberg, H. E., Hecobian, A., Knapp, D. J., Mikoviny,

T., Riemer, D., Sachse, G. W., Sessions, W., Weber, R. J., Weinheimer, A. J., Wisthaler, A., and Jimenez, J. L.: Effects of aging on organic aerosol from open biomass burning smoke in aircraft and laboratory studies, Atmos. Chem. Phys., 11, 12049–12064, doi:10.5194/acp-11-12049-2011, 2011.

Daellenbach, K. R., Bozzetti, C., Křepelová, A., Canonaco, F., Wolf, R., Huang, R.-J., Zotter, P., Crippa, M., Slowik, J. G., Zhang, Y., Szidat, S., Baltensperger, U., Prévôt, A. S. H., and El Haddad, I.: Characterization and source apportionment of organic aerosol using offline aerosol mass spectrometry, Atmos. Meas. Tech., in preparation, 2015.

DeCarlo, P. F., Kimmel, J. R., Trimborn, A., Northway, M. J., Jayne, J. T., Aiken, A. C., Gonin, M., Fuhrer, K., Horvath, T., Docherty, K. S., Worsnop, D. R., and Jimenez, J. L.: Field-deployable, high-resolution, time-of-flight aerosol mass spectrometer, Anal. Chem., 78, 8281–8289, 2006.

Docherty, K. S., Aiken, A. C., Huffman, J. A., Ulbrich, I. M., DeCarlo, P. F., Sueper, D., Worsnop, D. R., Snyder, D. C., Peltier, R. E., Weber, R. J., Grover, B. D., Eatough, D. J., Williams, B. J., Goldstein, A. H., Ziemann, P. J., and Jimenez, J. L.: The 2005 Study of Organic Aerosols at Riverside (SOAR-1): instrumental intercomparisons and fine particle composition, Atmos. Chem. Phys., 11, 12387–12420, doi:10.5194/acp-11-12387-2011, 2011.

Drewnick, F., Hings, S. S., DeCarlo, P., Jayne, J. T., Gonin, M., Fuhrer, K., Weimer, S., Jimenez, J. L., Demerjian, K. L., Borrmann, S., and Worsnop, D. R.: A new time-of-flight aerosol mass spectrometer (TOF-AMS) - Instrument description and first field deployment, Aerosol Sci. Tech., 39, 637–658, 2005.

Drinovec, L., Močnik, G., Zotter, P., Prévôt, A. S. H., Ruckstuhl, C., Coz, E., Rupakheti, M., Sciare, J., Müller, T., Wiedensohler, A., and Hansen, A. D. A.: The "dual-spot" Aethalometer: an improved measurement of aerosol black carbon with real-time loading compensation, Atmos. Meas. Tech., 8, 1965–1979, doi:10.5194/amt-8-1965-2015, 2015.

Faber, P., Drewnick, F., Veres, P. R., Williams, J., and Borrmann, S.: Anthropogenic sources of aerosol particles in a football stadium: Real-time characterization of emissions from cigarette smoking, cooking, hand flares, and color smoke bombs by high-resolution aerosol mass spectrometry, Atmos. Environ., 77, 1043–1051, 2013.

Favez, O., El Haddad, I., Piot, C., Boréave, A., Abidi, E., Marchand, N., Jaffrezo, J.-L., Besombes, J.-L., Personnaz, M.-B., Sciare, J., Wortham, H., George, C., and D'Anna, B.: Inter-comparison of source apportionment models for the estimation of wood burning aerosols during wintertime in an Alpine city (Grenoble, France), Atmos. Chem. Phys., 10, 5295–5314, doi:10.5194/acp-10-5295-2010, 2010.

Fröhlich, R., Cubison, M. J., Slowik, J. G., Bukowiecki, N., Prévôt, A. S. H., Baltensperger, U., Schneider, J., Kimmel, J. R., Gonin, M., Rohner, U., Worsnop, D. R., and Jayne, J. T.: The ToF-ACSM: a portable aerosol chemical speciation monitor with TOFMS detection, Atmos. Meas. Tech., 6, 3225–3241, doi:10.5194/amt-6-3225-2013, 2013.

Gaeggeler, K., Prevot, A., Dommen, J., Legreid, G., Reimann, S., and Baltensperger, U.: Residential wood burning in an Alpine valley as a source for oxygenated volatile organic compounds, hydrocarbons and organic acids, Atmos. Environ., 42, 8278–8287, 2008.

Graus, M., Müller, M., and Hansel, A.: High resolution PTR-TOF: Quantification and formula confirmation of VOC in real time, J. Am. Soc. Mass Spectrom., 21, 1037–1044, 2010.

Grieshop, A. P., Donahue, N. M., and Robinson, A. L.: Laboratory investigation of photochemical oxidation of organic aerosol from wood fires 2: analysis of aerosol mass spectrometer data, Atmos. Chem. Phys., 9, 2227–2240, doi:10.5194/acp-9-2227-2009, 2009.

Hallquist, M., Wenger, J. C., Baltensperger, U., Rudich, Y., Simpson, D., Claeys, M., Dommen, J., Donahue, N. M., George, C., Goldstein, A. H., Hamilton, J. F., Herrmann, H., Hoffmann, T., Iinuma, Y., Jang, M., Jenkin, M. E., Jimenez, J. L., Kiendler-Scharr, A., Maenhaut, W., McFiggans, G., Mentel, Th. F., Monod, A., Prévôt, A. S. H., Seinfeld, J. H., Surratt, J. D., Szmigielski, R., and Wildt, J.: The formation, properties and impact of secondary organic aerosol: current and emerging issues, Atmos. Chem. Phys., 9, 5155–5236, doi:10.5194/acp-9-5155-2009, 2009.

Hansel, A., Jordan, A., Holzinger, R., Prazeller, P., Vogel, W., and Lindinger, W.: Proton transfer reaction mass spectrometry: online trace gas analysis at the ppb level, Int. J. Mass Spectrom. Ion Processes, 149–150, 609–619, 1995.

Hansen, A., Rosen, H., and Novakov, T.: The aethalometer – An instrument for the real-time measurement of optical absorption by aerosol particles, Sci. Total Environ., 36, 191–196, 1984.

Heringa, M. F., DeCarlo, P. F., Chirico, R., Tritscher, T., Dommen, J., Weingartner, E., Richter, R., Wehrle, G., Prévôt, A. S. H., and Baltensperger, U.: Investigations of primary and secondary particulate matter of different wood combustion appliances with a high-resolution time-of-flight aerosol mass spectrometer, Atmos. Chem. Phys., 11, 5945–5957, doi:10.5194/acp-11-5945-2011, 2011.

Heringa, M. F., DeCarlo, P. F., Chirico, R., Lauber, A., Doberer, A., Good, J., Nussbaumer, T., Keller, A., Burtscher, H., Richard, A., Miljevic, B., Prevot, A. S. H., and Baltensperger, U.: Time-resolved characterization of primary emissions from residential wood combustion appliances, Environ. Sci. Technol., 46, 11418–11425, 2012.

Holzinger, R., Warneke, C., Hansel, A., Jordan, A., Lindinger, W., Scharffe, D. H., Schade, G., and Crutzen, P. J.: Biomass burning as a source of formaldehyde, acetaldehyde, methanol, acetone, acetonitrile, and hydrogen cyanide, Geophys. Res. Lett., 26, 1161–1164, 1999.

Hu, Q. H., Xie, Z. Q., Wang, X. M., Kang, H., and Zhang, P.: Levoglucosan indicates high levels of biomass burning aerosols over oceans from the Arctic to Antarctic, Sci. Rep., 3, 3119, doi:10.1038/srep03119, 2013a.

Hu, W. W., Hu, M., Yuan, B., Jimenez, J. L., Tang, Q., Peng, J. F., Hu, W., Shao, M., Wang, M., Zeng, L. M., Wu, Y. S., Gong, Z. H., Huang, X. F., and He, L. Y.: Insights on organic aerosol aging and the influence of coal combustion at a regional receptor site of central eastern China, Atmos. Chem. Phys., 13, 10095–10112, doi:10.5194/acp-13-10095-2013, 2013b.

Huang, R. J., Zhang, Y., Bozzetti, C., Ho, K. F., Cao, J. J., Han, Y., Daellenbach, K. R., Slowik, J. G., Platt, S. M., Canonaco, F., Zotter, P., Wolf, R., Pieber, S. M., Bruns, E. A., Crippa, M., Ciarelli, G., Piazzalunga, A., Schwikowski, M., Abbaszade, G., Schnelle-Kreis, J., Zimmermann, R., An, Z., Szidat, S., Baltensperger, U., El Haddad, I., and Prevot, A. S.: High secondary aerosol contri-

bution to particulate pollution during haze events in China, Nature, 514, 218–222, 2014.

Huffman, J. A., Jayne, J. T., Drewnick, F., Aiken, A. C., Onasch, T., Worsnop, D. R., and Jimenez, J. L.: Design, modeling, optimization, and experimental tests of a particle beam width probe for the Aerodyne aerosol mass spectrometer, Aerosol Sci. Technol., 39, 1143–1163, 2005.

ISO13528: Statistical Methods for Use in Proficiency Testing by Interlaboratory Comparisons, ISO 13528, International Organization for Standardization, Geneva, Switzerland, 2005.

Jacob, D. J., Field, B. D., Li, Q., Blake, D. R., de Gouw, J., Warneke, C., Hansel, A., Wisthaler, A., Singh, H. B., and Guenther, A.: Global budget of methanol: Constraints from atmospheric observations, J. Geophys. Res.-Atmos., 110, D08303, doi:10.1029/2004JD005172, 2005.

Jayne, J., Leard, D., Zhang, X., Davidovits, P., Smith, K., Kolb, C., and Worsnop, D.: Development of an aerosol mass spectrometer for size and composition analysis of submicron particles, Aerosol Sci. Tech., 33, 49–70, 2000.

Jimenez, J. L., Canagaratna, M. R., Donahue, N. M., Prévôt, A. S. H., Zhang, Q., Kroll, J. H., DeCarlo, P. F., Allan, J. D., Coe, H., Ng, N. L., Aiken, A. C., Docherty, K. S., Ulbrich, I. M., Grieshop, A. P., Robinson, A. L., Duplissy, J., Smith, J. D., Wilson, K. R., Lanz, V. A., Hueglin, C., Sun, Y. L., Tian, J., Laaksonen, A., Raatikainen, T., Rautiainen, J., Vaattovaara, P., Ehn, M., Kulmala, M., Tomlinson, J. M., Collins, D. R., Cubison, M. J., E., Dunlea, J., Huffman, J. A., Onasch, T. B., Alfarra, M. R., Williams, P. I., Bower, K., Kondo, Y., Schneider, J., Drewnick, F., Borrmann, S., Weimer, S., Demerjian, K., Salcedo, D., Cottrell, L., Griffin, R., Takami, A., Miyoshi, T., Hatakeyama, S., Shimono, A., Sun, J. Y., Zhang, Y. M., Dzepina, K., Kimmel, J. R., Sueper, D., Jayne, J. T., Herndon, S. C., Trimborn, A. M., Williams, L. R., Wood, E. C., Middlebrook, A. M., Kolb, C. E., Baltensperger, U., and Worsnop, D. R.: Evolution of organic aerosols in the atmosphere, Science, 326, 1525–1529, 2009.

Kanakidou, M., Seinfeld, J. H., Pandis, S. N., Barnes, I., Dentener, F. J., Facchini, M. C., Van Dingenen, R., Ervens, B., Nenes, A., Nielsen, C. J., Swietlicki, E., Putaud, J. P., Balkanski, Y., Fuzzi, S., Horth, J., Moortgat, G. K., Winterhalter, R., Myhre, C. E. L., Tsigaridis, K., Vignati, E., Stephanou, E. G., and Wilson, J.: Organic aerosol and global climate modelling: a review, Atmos. Chem. Phys., 5, 1053–1123, doi:10.5194/acp-5-1053-2005, 2005.

Karagulian, F. and Belis, C. A.: Enhancing source apportionment with receptor models to foster the air quality directive implementation, Int. J. Environ. Pollut., 50, 190–199, 2012.

Kimmel, J. R., Farmer, D. K., Cubison, M. J., Sueper, D., Tanner, C., Nemitz, E., Worsnop, D. R., Gonin, M., and Jimenez, J. L.: Real-time aerosol mass spectrometry with millisecond resolution, Int. J. Mass Spectrom., 303, 15–26, 2011.

Laden, F., Neas, L. M., Dockery, D. W., and Schwartz, J.: Association of fine particulate matter from different sources with daily mortality in six US cities, Environ. Health Persp., 108, 941–947, 2000.

Lanz, V. A., Alfarra, M. R., Baltensperger, U., Buchmann, B., Hueglin, C., and Prévôt, A. S. H.: Source apportionment of submicron organic aerosols at an urban site by factor analytical modelling of aerosol mass spectra, Atmos. Chem. Phys., 7, 1503–1522, doi:10.5194/acp-7-1503-2007, 2007.

Lanz, V. A., Alfarra, M. R., Baltensperger, U., Buchmann, B., Hueglin, C., Szidat, S., Wehrli, M. N., Wacker, L., Weimer, S., Caseiro, A., Puxbaum, H., and Prévôt, A. S. H.: Source attribution of submicron organic aerosols during wintertime inversions by advanced factor analysis of aerosol mass spectra, Environ. Sci. Tech., 42, 214–220, 2008.

Lanz, V. A., Prévôt, A. S. H., Alfarra, M. R., Weimer, S., Mohr, C., DeCarlo, P. F., Gianini, M. F. D., Hueglin, C., Schneider, J., Favez, O., D'Anna, B., George, C., and Baltensperger, U.: Characterization of aerosol chemical composition with aerosol mass spectrometry in Central Europe: an overview, Atmos. Chem. Phys., 10, 10453–10471, doi:10.5194/acp-10-10453-2010, 2010.

Li, Y. J., Lee, B. P., Su, L., Fung, J. C. H., and Chan, C.K.: Seasonal characteristics of fine particulate matter (PM) based on high-resolution time-of-flight aerosol mass spectrometric (HR-ToF-AMS) measurements at the HKUST Supersite in Hong Kong, Atmos. Chem. Phys., 15, 37–53, doi:10.5194/acp-15-37-2015, 2015.

Lim, S. S., Vos, T., Flaxman, A. D., Danaei, G., Shibuya, K., Adair-Rohani, H., AlMazroa, M. A., Amann, M., Anderson, H. R., Andrews, K. G., Aryee, M., Atkinson, C., Bacchus, L. J., Bahalim, A. N., Balakrishnan, K., Balmes, J., Barker-Collo, S., Baxter, A., Bell, M. L., Blore, J. D., Blyth, F., Bonner, C., Borges, G., Bourne, R., Boussinesq, M., Brauer, M., Brooks, P., Bruce, N. G., Brunekreef, B., Bryan-Hancock, C., Bucello, C., Buchbinder, R., Bull, F., Burnett, R. T., Byers, T. E., Calabria, B., Carapetis, J., Carnahan, E., Chafe, Z., Charlson, F., Chen, H., Chen, J. S., Cheng, A. T.-A., Child, J. C., Cohen, A., Colson, K. E., Cowie, B. C., Darby, S., Darling, S., Davis, A., Degenhardt, L., Dentener, F., Jarlais, D. C. D., Devries, K., Dherani, M., Ding, E. L., Dorsey, E. R., Driscoll, T., Edmond, K., Ali, S. E., Engell, R. E., Erwin, P. J., Fahimi, S., Falder, G., Farzadfar, F., Ferrari, A., Finucane, M. M., Flaxman, S., Fowkes, F. G. R., Freedman, G., Freeman, M. K., Gakidou, E., Ghosh, S., Giovannucci, E., Gmel, G., Graham, K., Grainger, R., Grant, B., Gunnell, D., Gutierrez, H. R., Hall, W., Hoek, H. W., Hogan, A., Hosgood III, H. D., Hoy, D., Hu, H., Hubbell, B. J., Hutchings, S. J., Ibeanusi, S. E., Jacklyn, G. L., Jasrasaria, R., Jonas, J. B., Kan, H., Kanis, J. A., Kassebaum, N., Kawakami, N., Khang, Y.-H., Khatibzadeh, S., Khoo, J.-P., Kok, C., Laden, F., Lalloo, R., Lan, Q., Lathlean, T., Leasher, J. L., Leigh, J., Li, Y., Lin, J. K., Lipshultz, S. E., London, S., Lozano, R., Lu, Y., Mak, J., Malekzadeh, R., Mallinger, L., Marcenes, W., March, L., Marks, R., Martin, R., McGale, P., McGrath, J., Mehta, S., Memish, Z. A., Mensah, G. A., Merriman, T. R., Micha, R., Michaud, C., Mishra, V., Hanafiah, K. M., Mokdad, A. A., Morawska, L., Mozaffarian, D., Murphy, T., Naghavi, M., Neal, B., Nelson, P. K., Nolla, J. M., Norman, R., Olives, C., Omer, S. B., Orchard, J., Osborne, R., Ostro, B., Page, A., Pandey, K. D., Parry, C. D., Passmore, E., Patra, J., Pearce, N., Pelizzari, P. M., Petzold, M., Phillips, M. R., Pope, D., Pope III, C. A., Powles, J., Rao, M., Razavi, H., Rehfuess, E. A., Rehm, J. T., Ritz, B., Rivara, F. P., Roberts, T., Robinson, C., Rodriguez-Portales, J. A., Romieu, I., Room, R., Rosenfeld, L. C., Roy, A., Rushton, L., Salomon, J. A., Sampson, U., Sanchez-Riera, L., Sanman, E., Sapkota, A., Seedat, S., Shi, P., Shield, K., Shivakoti, R., Singh, G. M., Sleet, D. A., Smith, E., Smith, K. R., Stapelberg, N. J., Steenland, K., Stöckl, H., Stovner, L. J., Straif, K., Straney, L., Thurston, G. D.,

Tran, J. H., Dingenen, R. V., van Donkelaar, A., Veerman, J. L., Vijayakumar, L., Weintraub, R., Weissman, M. M., White, R. A., Whiteford, H., Wiersma, S. T., Wilkinson, J. D., Williams, H. C., Williams, W., Wilson, N., Woolf, A. D., Yip, P., Zielinski, J. M., Lopez, A. D., Murray, C. J., and Ezzati, M.: A comparative risk assessment of burden of disease and injury attributable to 67 risk factors and risk factor clusters in 21 regions, 1990–2010: a systematic analysis for the Global Burden of Disease Study 2010, Lancet, 380, 2224–2260, 2013.

Liu, D., Allan, J. D., Young, D. E., Coe, H., Beddows, D., Fleming, Z. L., Flynn, M. J., Gallagher, M. W., Harrison, R. M., Lee, J., Prevot, A. S. H., Taylor, J. W., Yin, J., Williams, P. I., and Zotter, P.: Size distribution, mixing state and source apportionment of black carbon aerosol in London during wintertime, Atmos. Chem. Phys., 14, 10061–10084, doi:10.5194/acp-14-10061-2014, 2014.

Liu, P., Ziemann, P. J., Kittelson, D. B., and McMurry, P. H.: Generating particle beams of controlled dimensions and divergence: II. experimental evaluation of particle motion in aerodynamic lenses and nozzle expansions, Aerosol Sci. Tech., 22, 314–324, 1995a.

Liu, P., Ziemann, P. J., Kittelson, D. B., and McMurry, P. H.: Generating particle beams of controlled dimensions and divergence: I. theory of particle motion in aerodynamic lenses and nozzle expansions, Aerosol Sci. Tech., 22, 293–313, 1995b.

Liu, P. S. K., Deng, R., Smith, K. A., Williams, L. R., Jayne, J. T., Canagaratna, M. R., Moore, K., Onasch, T. B., Worsnop, D. R., and Deshler, T.: Transmission efficiency of an aerodynamic focusing lens system: comparison of model calculations and laboratory measurements for the Aerodyne aerosol mass spectrometer, Aerosol Sci. Tech., 41, 721–733, 2007.

Lohmann, U. and Feichter, J.: Global indirect aerosol effects: a review, Atmos. Chem. Phys., 5, 715–737, doi:10.5194/acp-5-715-2005, 2005.

Mahowald, N.: Aerosol indirect effect on biogeochemical cycles and climate, Science, 334, 794–796, 2011.

Mathers, C. D., Fat, D. M., Inoue, M., Rao, C., and Lopez, A. D.: Counting the dead and what they died from: an assessment of the global status of cause of death data, B. World Health Organ., 83, 171–177, 2005.

Matthew, B. M., Middlebrook, A. M., and Onasch, T. B.: Collection efficiencies in an Aerodyne aerosol mass spectrometer as a function of particle phase for laboratory generated aerosols, Aerosol Sci. Tech., 42, 884–898, 2008.

Mercado, L. M., Bellouin, N., Sitch, S., Boucher, O., Huntingford, C., Wild, M., and Cox, P. M.: Impact of changes in diffuse radiation on the global land carbon sink, Nature, 458, 1014–1017, 2009.

Mohr, C., Huffman, J. A., Cubison, M. J., Aiken, A. C., Docherty, K. S., Kimmel, J. R., Ulbrich, I. M., Hannigan, M., and Jimenez, J. L.: Characterization of primary organic aerosol emissions from meat cooking, trash burning, and motor vehicles with high-resolution aerosol mass spectrometry and comparison with ambient and chamber observations, Environ. Sci. Technol., 43, 2443–2449, doi:10.1021/es8011518, 2009.

Mohr, C., DeCarlo, P. F., Heringa, M. F., Chirico, R., Slowik, J. G., Richter, R., Reche, C., Alastuey, A., Querol, X., Seco, R., PeÑuelas, J., Jiménez, J. L., Crippa, M., Zimmermann, R., Baltensperger, U., and Prévôt, A. S. H.: Identification and quantification of organic aerosol from cooking and other sources in Barcelona using aerosol mass spectrometer data, Atmos. Chem. Phys., 12, 1649–1665, doi:10.5194/acp-12-1649-2012, 2012.

Ng, N. L., Canagaratna, M. R., Zhang, Q., Jimenez, J. L., Tian, J., Ulbrich, I. M., Kroll, J. H., Docherty, K. S., Chhabra, P. S., Bahreini, R., Murphy, S. M., Seinfeld, J. H., Hildebrandt, L., Donahue, N. M., DeCarlo, P. F., Lanz, V. A., Prévôt, A. S. H., Dinar, E., Rudich, Y., and Worsnop, D. R.: Organic aerosol components observed in Northern Hemispheric datasets from Aerosol Mass Spectrometry, Atmos. Chem. Phys., 10, 4625–4641, doi:10.5194/acp-10-4625-2010, 2010.

Ng, N. L., Canagaratna, M. R., Jimenez, J. L., Chhabra, P. S., Seinfeld, J. H., and Worsnop, D. R.: Changes in organic aerosol composition with aging inferred from aerosol mass spectra, Atmos. Chem. Phys., 11, 6465–6474, doi:10.5194/acp-11-6465-2011, 2011a.

Ng, N. L., Canagaratna, M. R., Jimenez, J. L., Zhang, Q., Ulbrich, I. M., and Worsnop, D. R.: Real-time methods for estimating organic component mass concentrations from aerosol mass spectrometer data, Environ. Sci. Technol., 45, 910–916, 2011b.

Ng, N. L., Herndon, S. C., Trimborn, A., Canagaratna, M. R., Croteau, P. L., Onasch, T. B., Sueper, D., Worsnop, D. R., Zhang, Q., Sun, Y. L., and Jayne, J. T.: An aerosol chemical speciation monitor (ACSM) for routine monitoring of the composition and mass concentrations of ambient aerosol, Aerosol Sci. Tech., 45, 780–794, 2011c.

Ovadnevaite, J., Ceburnis, D., Canagaratna, M., Berresheim, H., Bialek, J., Martucci, G., Worsnop, D. R., and O'Dowd, C.: On the effect of wind speed on submicron sea salt mass concentrations and source fluxes, J. Geophys. Res.-Atmos., 117, D16201, doi:10.1029/2011jd017379, 2012.

Paatero, P.: Least squares formulation of robust non-negative factor analysis, Chemometr. Intell. Lab., 37, 23–35, 1997.

Paatero, P.: The multilinear engine – a table-driven, least squares program for solving multilinear problems, including the n-way parallel factor analysis model, J. Comput. Graph. Stat., 8, 854–888, 1999.

Paatero, P. and Hopke, P. K.: Rotational tools for factor analytic models, J. Chemometr., 23, 91–100, 2009.

Paatero, P. and Tapper, U.: Positive matrix factorization: a non-negative factor model with optimal utilization of error estimates of data values, Environmetrics, 5, 111–126, 1994.

Paatero, P., Eberly, S., Brown, S. G., and Norris, G. A.: Methods for estimating uncertainty in factor analytic solutions, Atmos. Meas. Tech., 7, 781–797, doi:10.5194/amt-7-781-2014, 2014.

Petit, J.-E., Favez, O., Sciare, J., Crenn, V., Sarda-Estève, R., Bonnaire, N., Močnik, G., Dupont, J.-C., Haeffelin, M., and Leoz-Garziandia, E.: Two years of near real-time chemical composition of submicron aerosols in the region of Paris using an Aerosol Chemical Speciation Monitor (ACSM) and a multi-wavelength Aethalometer, Atmos. Chem. Phys., 15, 2985–3005, doi:10.5194/acp-15-2985-2015, 2015

Pope, C. A. and Dockery, D. W.: Health effects of fine particulate air pollution: lines that connect, J. Air Waste Manage., 56, 709–742, 2006.

Saleh, R., Hennigan, C. J., McMeeking, G. R., Chuang, W. K., Robinson, E. S., Coe, H., Donahue, N. M., and Robinson, A. L.: Absorptivity of brown carbon in fresh and photo-chemically aged biomass-burning emissions, Atmos. Chem. Phys., 13, 7683–7693, doi:10.5194/acp-13-7683-2013, 2013.

Sandradewi, J., Prévôt, A. S., Szidat, S., Perron, N., Alfarra, M. R., Lanz, V. A., Weingartner, E., and Baltensperger, U.: Using aerosol light absorption measurements for the quantitative determination of wood burning and traffic emission contributions to particulate matter, Environ. Sci. Technol., 42, 3316–3323, 2008.

Sciare, J., d'Argouges, O., Sarda-Estève, R., Gaimoz, C., Dolgorouky, C., Bonnaire, N., Favez, O., Bonsang, B., and Gros, V.: Large contribution of water-insoluble secondary organic aerosols in the region of Paris (France) during wintertime, J. Geophys. Res.-Atmos., 116, D22203, doi:10.1029/2011jd015756, 2011.

Seaton, A., Godden, D., MacNee, W., and Donaldson, K.: Particulate air pollution and acute health effects, Lancet, 345, 176–178, 1995.

Simoneit, B., Schauer, J., Nolte, C., Oros, D., Elias, V., Fraser, M., Rogge, W., and Cass, G.: Levoglucosan, a tracer for cellulose in biomass burning and atmospheric particles, Atmos. Environ., 33, 173–182, 1999.

Slowik, J. G., Vlasenko, A., McGuire, M., Evans, G. J., and Abbatt, J. P. D.: Simultaneous factor analysis of organic particle and gas mass spectra: AMS and PTR-MS measurements at an urban site, Atmos. Chem. Phys., 10, 1969–1988, doi:10.5194/acp-10-1969-2010, 2010.

Stevens, B. and Feingold, G.: Untangling aerosol effects on clouds and precipitation in a buffered system, Nature, 461, 607–613, 2009.

Sun, J., Zhang, Q., Canagaratna, M. R., Zhang, Y., Ng, N. L., Sun, Y., Jayne, J. T., Zhang, X., Zhang, X., and Worsnop, D. R.: Highly time- and size-resolved characterization of submicron aerosol particles in Beijing using an Aerodyne aerosol mass spectrometer, Atmos. Environ., 44, 131–140, 2010.

Sun, Y.-L., Zhang, Q., Schwab, J. J., Demerjian, K. L., Chen, W.-N., Bae, M.-S., Hung, H.-M., Hogrefe, O., Frank, B., Rattigan, O. V., and Lin, Y.-C.: Characterization of the sources and processes of organic and inorganic aerosols in New York city with a high-resolution time-of-flight aerosol mass spectrometer, Atmos. Chem. Phys., 11, 1581–1602, doi:10.5194/acp-11-1581-2011, 2011.

Timonen, H., Carbone, S., Aurela, M., Saarnio, K., Saarikoski, S., Ng, N. L., Canagaratna, M. R., Kulmala, M., Kerminen, V.-M., Worsnop, D. R., and Hillamo, R.: Characteristics, sources and water-solubility of ambient submicron organic aerosol in springtime in Helsinki, Finland, J. Aerosol Sci., 56, 61–77, 2013.

Ulbrich, I. M., Canagaratna, M. R., Zhang, Q., Worsnop, D. R., and Jimenez, J. L.: Interpretation of organic components from Positive Matrix Factorization of aerosol mass spectrometric data, Atmos. Chem. Phys., 9, 2891–2918, doi:10.5194/acp-9-2891-2009, 2009.

Wang, Y., Wang, M., Zhang, R., Ghan, S. J., Lin, Y., Hu, J., Pan, B., Levy, M., Jiang, J. H., and Molina, M. J.: Assessing the effects of anthropogenic aerosols on Pacific storm track using a multiscale global climate model, P. Natl. Acad. Sci. USA, 111, 6894–6899, 2014a.

Wang, Y., Zhang, R., and Saravanan, R.: Asian pollution climatically modulates mid-latitude cyclones following hierarchical modelling and observational analysis, Nat. Commun., 5, 3098, doi:10.1038/ncomms4098, 2014b.

Watson, J. G., Robinson, N. F., Lewis, C., Coulter, T., Chow, J. C., Fujita, E. M., Lowenthal, D., Conner, T. L., Henry, R. C., and Willis, R. D.: Chemical Mass Balance Receptor Model Version 8 (CMB8) User's Manual, Prepared for US Environmental Protection Agency, Research Triangle Park, NC, by Desert Research Institute, Reno, NV, 1997.

Weimer, S., Alfarra, M. R., Schreiber, D., Mohr, M., Prévôt, A. S. H., and Baltensperger, U.: Organic aerosol mass spectral signatures from wood-burning emissions: influence of burning conditions and wood type, J. Geophys. Res.-Atmos., 113, D10304, doi:10.1029/2007jd009309, 2008.

Yin, J., Cumberland, S. A., Harrison, R. M., Allan, J., Young, D. E., Williams, P. I., and Coe, H.: Receptor modelling of fine particles in southern England using CMB including comparison with AMS-PMF factors, Atmos. Chem. Phys., 15, 2139–2158, doi:10.5194/acp-15-2139-2015, 2015.

Young, D. E., Allan, J. D., Williams, P. I., Green, D. C., Harrison, R. M., Yin, J., Flynn, M. J., Gallagher, M. W., and Coe, H.: Investigating a two-component model of solid fuel organic aerosol in London: processes, PM_1 contributions, and seasonality, Atmos. Chem. Phys., 15, 2429–2443, doi:10.5194/acp-15-2429-2015, 2015.

Zhang, Q., Alfarra, M. R., Worsnop, D. R., Allan, J. D., Coe, H., Canagaratna, M. R., and Jimenez, J. L.: Deconvolution and quantification of hydrocarbon-like and oxygenated organic aerosols based on aerosol mass spectrometry, Environ. Sci. Technol., 39, 4938–4952, doi:10.1021/es048568l, 2005a.

Zhang, Q., Worsnop, D. R., Canagaratna, M. R., and Jimenez, J. L.: Hydrocarbon-like and oxygenated organic aerosols in Pittsburgh: insights into sources and processes of organic aerosols, Atmos. Chem. Phys., 5, 3289–3311, doi:10.5194/acp-5-3289-2005, 2005b.

Zhang, Q., Jimenez, J. L., Canagaratna, M. R., Ulbrich, I. M., Ng, N. L., Worsnop, D. R., and Sun, Y.: Understanding atmospheric organic aerosols via factor analysis of aerosol mass spectrometry: a review, Anal. Bioanal. Chem., 401, 3045–3067, 2011.

Zhang, X., Smith, K. A., Worsnop, D. R., Jimenez, J. L., Jayne, J. T., Kolb, C. E., Morris, J., and Davidovits, P.: Numerical characterization of particle beam collimation: part II integrated aerodynamic-lens–nozzle system, Aerosol Sci. Tech., 38, 619–638, 2004.